

1 Long-term chemical characterization of tropical and marine 2 aerosols at the CVAO from 2007 to 2011

3

4 **Khanneh Wadinga Fomba, Konrad Müller, Dominik van Pinxteren, Laurent**
5 **Poulain, Manuela van Pinxteren and Hartmut Herrmann**

6 TROPOS – Leibniz Institute for Tropospheric Research, Permoserstr. 15, 04318 Leipzig,
7 Germany

8 Corresponding author: Hartmut Herrmann (herrmann@tropos.de)

9

10

11 **Abstract**

12 The first long-term aerosol sampling and chemical characterization results from measurements at
13 the Cape Verde Atmospheric Observatory (CVAO) on the island of São Vicente are presented
14 and are discussed with respect to air mass origin and seasonal trends. In total 671 samples were
15 collected using a high volume PM₁₀ sampler on quartz fiber filters from January 2007 to
16 December 2011. The samples were analyzed for their aerosol chemical composition including
17 their ionic and organic constituents. Back trajectory analyses showed that the aerosol at CVAO
18 was strongly influenced by emissions from Europe and Africa with the later often responsible for
19 high mineral dust loading. Sea salt and mineral dust dominated the aerosol mass and made up in
20 total about 80% of the aerosol mass. The 5 year PM₁₀ mean was $47.1 \pm 55.5 \mu\text{g}/\text{m}^3$ while the
21 mineral dust and sea salt means were $27.9 \pm 48.7 \mu\text{g}/\text{m}^3$ and $11.1 \pm 5.5 \mu\text{g}/\text{m}^3$, respectively. Non-
22 sea-salt (nss) sulfate made up 62 % of the total sulfate and originated from both long range
23 transport from Africa or Europe and marine sources. Strong seasonal variation was observed for
24 the aerosol components. While nitrate showed no clear seasonal variation with an annual mean of
25 $1.1 \pm 0.6 \mu\text{g}/\text{m}^3$, the aerosol mass, OC (Organic Carbon) and EC (Elemental Carbon), showed
26 strong winter maxima due to strong influence of African air mass inflow. Additionally during
27 summer, elevated concentrations of OM were observed originating from marine emissions. A
28 summer maximum was observed for non-sea-salt sulfate and was connected to periods when air

29 mass inflow was predominantly of marine origin indicating that marine biogenic emissions were
30 a significant source. Ammonium showed a distinct maximum in spring and coincided with ocean
31 surface water chlorophyll *a* concentrations. Good correlations were also observed between nss-
32 sulfate and oxalate during the summer and winter seasons indicating a likely photochemical in-
33 cloud processing of the marine and anthropogenic precursors of these species. High temporal
34 variability was observed in both chloride and bromide depletion differing significantly within the
35 seasons, air mass history and Saharan dust concentration. Chloride (bromide) depletion varied
36 from 8.8 ± 8.5 % (62 ± 42 %) in Saharan dust dominated air mass to 30 ± 12 % (87 ± 11 %) in
37 polluted Europe air masses. During summer, bromide depletion often reached 100 % in marine as
38 well as in polluted continental samples. In addition to the influence of the aerosol acidic
39 components, photochemistry was one of the main drivers of halogenide depletion during the
40 summer while during dust events, displacement reaction with nitric acid was found to be the
41 dominant mechanism. PMF analysis identified three major aerosol sources including sea salt,
42 aged sea salt and long range transport. The ionic budget was dominated by the first two of these
43 factors while the long range transport factor could only account for about 14 % of the total
44 observed ionic mass.

45 **Key words:** PM₁₀ aerosol, seasonality, chemical composition, Saharan dust, halogenide
46 depletion

47

48

49

50

51

52

53

54

55

56

57 **1. Introduction**

58 The interest in research on atmospheric aerosols is not only limited to heavily polluted megacities
59 and other strongly anthropogenically polluted areas but also concerns naturally mobilized dust
60 and sea-salt aerosols which are in the focus of marine chemistry, biology and atmospheric
61 chemistry (Raes et al., 2010; Radhi et al., 2010; Heller and Croot, 2011; Carpenter et al., 2004;
62 Quinn and Bates, 2005; Formenti et al., 2011). The creation and operation of the Cape Verde
63 Atmospheric Observatory (Observatório Atmosférico de Cabo Verde: Humberto Duarte
64 Fonseca, CVAO) in 2006 located at the São Vicente island was a joint activity of British, German
65 and Cape Verdean scientific institutes with funding from the European Union (EU), national
66 scientific projects and institutions. On the one hand, the CVAO is downwind of the Mauritanian
67 coastal upwelling region off northwest Africa, an area of high marine biological productivity.
68 Observations made at the CVAO therefore provide information on links between atmospheric
69 compositional changes, marine biology and climate. On the other hand, satellite, ground-based,
70 ship and aircraft measurements have shown the outflow of Saharan dust into the Atlantic Ocean
71 usually across the Cape Verde islands (Chiapello et al., 1999; Formenti et al., 2003; Reid et al.,
72 2003; Tesche et al., 2011; Gelado-Caballero et al., 2012) making it a suitable location for
73 characterizing mineral dust. The station is situated at the far edge of the island in the direction of
74 air mass inflow to the island so that air masses observed at the station are free from local
75 pollution thereby making the station suitable for also performing remote marine aerosol
76 experiments. The atmospheric deposition of nutrients that are derived from dust such as nitrogen,
77 phosphorus and iron compounds into the oceans plays a crucial role in marine biogeochemical
78 cycles and in some areas establishes a major nutrient input to the open oceans (Cropp et al., 2005;
79 Ohde and Siegel, 2010; Bates et al., 2001). The role of desert aerosols in atmospheric processes
80 strongly depends on a variety of physicochemical parameters and their spatial distribution and
81 transformations in the atmosphere (Kelly et al., 2007; Lee et al., 2010).

82 During late spring and summer, the CVAO site mostly receives North Atlantic marine air masses
83 along the NNE trade winds which, although, are sometimes influenced by the Mauritanian
84 upwelling, provide the possibility for long-term studies of “background” Atlantic air and its
85 associated trace gases of oceanic origin. During late fall and winter, Cape Verde is situated in the
86 direct transport pathway of Saharan dust from Africa to the North Atlantic. During this season
87 dust is transported in the lower troposphere and the deposition takes place mainly over the eastern

88 tropical Atlantic (Schepanski et al., 2009) and Cape Verde.
89 In principle, atmospheric chemistry in this region of the Cape Verde Islands is expected to be
90 influenced by emissions from the ocean (Mahajan et al., 2010; Read et al., 2008), Saharan dust,
91 anthropogenically released gases and particles from continental Africa, south-western Europe and
92 in minor cases North-American sources.

93 The investigation of the role of mineral dust in the ocean has been the focus of a number of
94 research and ship cruises along the tropical Atlantic oceans (Bates et al., 2001; Chen and Siefert,
95 2003; Allan et al., 2009). However, these measurements have mostly focused on short term
96 measurements during intensive field campaigns that last for 3-6 weeks, making predictions about
97 seasonal variability and long term understanding of atmospheric processes quite difficult. Such
98 long-term data sets have been often requested (Mahowald et al., 2005) but only a few data
99 actually exist for the region of the tropical North Atlantic (e.g., (Kandler et al., 2007; Chiapello et
100 al., 1995). Chiapello et al. (1995) collected filter samples over three years for metal analyses at
101 the Cape Verde island Sal from a region that was far from the coastline and influenced by the
102 island itself. There are also some data from ship cruises and short term experiments near this
103 region (Chen and Siefert, 2004; Rijkenberg et al., 2008; Kandler et al., 2011). Long-term
104 observations were made in the subtropical region at Izaña (Tenerife) 1500 km NNE from São
105 Vicente but Izaña is located at 2373 m a.s.l. and Santa Cruz is influenced heavily by local
106 pollution (Alastuey et al., 2005). Long-term measurements in a remote site in the north-eastern
107 tropical Atlantic Ocean are not known. In a recent study (Schulz et al., 2012), a marine
108 atmospheric monitoring network for long-term observations of dust transport and deposition to
109 the ocean was asked for as well as encouraged for future harmonized activities in marine aerosol
110 research. The measurements at the CVAO intend to improve on the present data scarcity and also
111 meet other expectations.

112 Within the present study the long-term PM₁₀ high volume filter measurements at the CVAO are
113 discussed. The presented results aim to deliver the first long-term data set of aerosol chemical
114 composition for further use, e.g. in marine biogeochemistry research and for marine aerosol
115 modeling where long-term experimental data on the aerosol constitution and its size-resolved
116 chemical composition are needed. The results are focused on samples collected since the creation
117 of the CVAO in 2007 until the end of 2011. The aspects addressed are particulate mass
118 concentrations, chloride depletion, concentration of ionic components, organic matter (OM) and
119 EC. The mineral dust fraction of the aerosol particles and its seasonal and inter-annual variability

120 are also discussed. Back trajectories were used to classify typical source regions. Related works
121 from the CVAO include first investigations from short term experiments of PM characterization
122 (Muller et al., 2010; Fomba et al., 2013; Müller et al., 2010) and of specific organic single
123 compounds (Müller et al., 2009).

124

125 **2. Experimental**

126 **2.1 Site and sampling**

127 Sampling was done at the CVAO which is located at the north-eastern shore of the island of São
128 Vicente in Cape Verde. The sampling site is situated 70 m from the coastline (16° 51' 49 N, 24°
129 52' 02 W) about 10 m above sea level (asl). This region experiences constant north-eastern winds
130 from Africa through the Canary Islands. The average annual temperature at the CVAO is $23.6 \pm$
131 4.0°C and it is an arid region with a maximum of 24-350 mm rainfall per year. The precipitation
132 frequency is about 3 to 10 events per year mainly between August and October. Therefore, the
133 wet deposition of particles in this region is negligible. A more detailed description of the
134 meteorological conditions can be found (Carpenter et al., 2010). Sample collection was
135 performed on top of a tower with an inlet height of 32 m to reduce the direct influence of sea
136 spray on the collected particles. Due to the location of the station, influences from the island like
137 orographic influences in dust sedimentation and anthropogenic emissions are negligible. Thus the
138 collected samples are representative of a clean atmosphere over the ocean and not contaminated
139 by gases or particulates from the island itself. However, though such events are very rare, during
140 southwesterly winds influences from the island could be observed.

141 All background meteorological data, temperature, relative humidity, and wind measurements
142 were collected from 31 m and from 10 m heights at a frequency of 1 Hz, then averaged over one
143 minute and ten minutes to hourly values. Atmospheric pressure and broadband UV radiation were
144 recorded at a 4 m height.

145 Particle sampling was done using a high volume (HV) collector with a PM₁₀-inlet (Digitel filter
146 sampler DHA-80, Walter Riemer Messtechnik, Germany) that was operated with an average flow
147 rate of 500 l/min in a 24 h sampling period during intensive campaigns and was switched to 72 h
148 sampling period, otherwise. The high volume samples were collected on acquired 150 mm pre-
149 heated quartz fiber filters (Munktell, MK 360) and were further pre-heated in our laboratory at

150 110 °C for 24 h to get rid of the OC background content. Our unpublished results of tests at
151 higher temperatures delivered similar blanks but the mechanical stability of the filters (abrasion
152 and breaking resistance) was better when handling at 110°C.

153 After sampling the filters were stored at 5 °C and subsequently cooled and transported to a
154 freezer. The long term storage and transportation of the collected filters from the CVAO to
155 Germany was always carried out in aluminum boxes at -20 °C.

156

157 **2.2 Laboratory Analysis**

158 The filters were equilibrated for 72 h under constant temperature (20 ± 1 °C) and humidity ($50 \pm$
159 5%) before and after collection and weighed using a microbalance (Mod. AT261 Delta Range,
160 Mettler-Toledo, Switzerland) with a reading precision of 10 µg.

161 For ion analysis, 25 % of the PM₁₀ quartz fiber filter was extracted with 30 ml MilliQ-water
162 (>18 MΩ cm, 15 min shaker, 15 min ultrasonic bath, 15 min shaker). Sample extracts were
163 filtered through a 0.45 µm one-way syringe filter to remove insoluble materials prior to ion
164 analysis. The ion analysis was performed for cations Na⁺, NH₄⁺, K⁺, Mg²⁺, Ca²⁺ and anions Cl⁻,
165 Br⁻, NO₃⁻, SO₄²⁻ and C₂O₄²⁻ using a standard ion-chromatography technique (ICS3000, DIONEX,
166 USA) equipped with an automatic eluent generation (KOH for anions and methanesulfonic acid
167 (MSA) for cations) and a micro-membrane suppression unit. For the anion separation a
168 combination of AG18 and AS18 (2 mm) was applied while for the cation separation CG16 and
169 CS16 (3 mm) were used. Chromatographic calibrations were carried out daily using a four point
170 standard (Fluka, Switzerland). The detection limits for all ions measured by conductivity
171 detection were within 0.002 µg/m³ except for calcium that was 0.02 µg/m³. Bromide was detected
172 using UV/VIS detection (VWD-1, Dionex) with a detection limit of 0.001 µg/m³. Analyzed field
173 blank filters were used for blank correction via subtraction. Non-sea salt sulfate (nss-sulfate) was
174 determined from the subtraction of sea salt sulfate (ss-sulfate) from the total sulfate. Ss-sulfate
175 was determined from the stable ratio $SO_4^{2-}/Na^+=0.251$ (Liebezeit, 2011) in sea water under the
176 assumption that sodium has no other sources.

177 Organic and elemental carbon were analyzed by a two-step thermographic method (C-mat 5500,
178 Ströhlein, Germany) with NDIR detection as described in the following literature (Neusüss et al.,
179 2002; Gnauk et al., 2008; Carpenter et al., 2010). The detection limits for quartz fiber filter
180 analysis were 30 ng/m³ for EC and 100 ng/m³ for OC. For the determination of OM (organic

181 matter) the estimation of Turpin (Turpin et al., 2000) was applied with OM considered as twice
182 OC ($OM = OC * 2$) which is recommended for aged aerosols. In previous studies, results of
183 single organic compounds were presented ((Müller et al., 2009; Alastuey et al., 2005; Müller et
184 al., 2010) while in the present work, only oxalic acid concentrations shall be discussed.

185 Air mass back trajectory analyses were performed to assist in the data interpretation and to
186 provide useful hints on various air mass origins. Back trajectories ensembles (van Pinxteren et al.,
187 2010) were calculated (starting 500m above ground) using the NOAA HYSPLIT (HYbrid Single-
188 Particle Lagrangian Integrated Trajectory, <http://www.arl.noaa.gov/ready/hysplit4.html>) model.

189

190 **2.3 Positive Matrix Factorization (PMF) Analysis**

191 Source apportionment of the analyzed aerosol chemical composition (OC, EC, Na^+ , NH_4^+ , K^+ ,
192 Mg^{2+} , Ca^{2+} , Cl^- , Br^- , NO_3^- , SO_4^{2-} and $C_2O_4^{2-}$) was performed using the multilinear Engine
193 algorithm (ME-2) developed by (Paatero, 1999)). Results were analyzed according to the ME-2
194 graphic interphase Sofi from (Canonaco et al., 2013)). Since PMF is a weighted least square
195 method, individual estimates of uncertainties associated with each data value are required. In this
196 work the uncertainties were obtained from the calibration uncertainties of the main ions and
197 OC/EC that were applied on the measured concentrations. The PMF was run using 2 to 5 factors
198 and each factor solution was evaluated using the seed. It was found that the 3 factors solution
199 could explain the data most appropriately and thus provided the most meaningful results (Figure
200 SI-2 in the supplementary information). The obtained solution was interpreted on the basis of the
201 air mass back trajectories, the meteorological conditions and the chemical composition of the
202 filters. Further details on the results of the different factors could be found in the supplementary
203 information (SI).

204

205 **3. Results**

206 **3.1 Back trajectory analysis**

207

208 *Please insert Figure 1 here*

209

210 Hourly back trajectory analyses were performed for more than 600 samples. In general, 96 h back
211 trajectory ensembles were calculated. The plots represent a trajectory ensemble consisting of 648
212 single back trajectories calculated for a 24 hour time interval of the individual samples. For a few
213 sampling periods longer back trajectories were calculated for a better understanding of possible
214 sources since submicron particles could have longer atmospheric lifetimes (Jaenicke, 1980)
215 depending on the height (Williams et al., 2002). The most important air mass origins were
216 classified as follows (Fig. 1):

217 (A) The air mass spent the last 96 h over the Atlantic Ocean and was from the northern or
218 northwestern Atlantic Ocean (16.5 % of all samples).

219 (B) The air mass spent less than 48 h over the Ocean in the last 96 hours before arriving at
220 CVAO and originated from the African continent crossing over the Saharan Desert, urban sites
221 (Nouakchott, Dakar, etc.) as well as biomass burning regions through the Mauritanian upwelling
222 region to the CVAO (22.2 % of all samples).

223 (C) Air masses from the Atlantic Ocean crossing the Mauritanian upwelling region, partially NW
224 Africa, Canary Islands (26.3 % of all samples).

225 (D) Air masses which originated from or in SW Europe and crossed the Mauritanian upwelling
226 region, coastal areas in NW Africa and/or the Canary Islands and the north-eastern Atlantic
227 Ocean (17.7 % of all samples).

228 (E) All further back trajectories (17.3 % of all samples) that could not be assigned to the above
229 four major classes. This include air masses that reached the CVAO from western Africa (south of
230 the Sahara), the equatorial Atlantic Ocean and from North-America.

231 Late fall and winter are the typical dust seasons at the Cape Verde islands. During this time
232 easterly and northeasterly winds transport Saharan dust into the tropical eastern Atlantic. During
233 spring and summer, the air mass origin is mainly marine but sometimes the trade winds cross the
234 African coast in Morocco and Western Sahara and at times originate from the Iberian Peninsula.
235 Equatorial air masses rarely reach the Cape Verde archipelago.

236 **3.2 Chemical characterization of the aerosol constituents**

237 671 samples were collected and analyzed for their chemical composition over the stated time
238 period. Table 1 shows the overview of the total number of investigated samples in this work
239 during the investigated time period. The observed difference in the number of collected filters
240 between the years is related to the different sampling routines that were implemented. During the

241 first four months of sampling in 2007, the samples were collected as 72 hours samples within one
242 week in the regime 3 h sampling and 4 h sampling break. After the first intensive campaign
243 (May/June 2007) during which sample collection was done for 24 h without a break between
244 filter sampling, the collection was changed to 3 days continuous sampling and 3 days pause
245 within the time period of August 2007 and December 2008. Afterwards the sampling period was
246 fixed at 72 h without a break. A few exceptions to this sampling regime were caused by power
247 failures at the CVAO and sampler defect in July/August 2009 (cf. Table 1). This explains the
248 higher number of filters observed in 2009 to 2011 in comparison to 2007 and 2008. From
249 October 2009 to July 2010 samples were collected on top of a container due to the reconstruction
250 of the tower. At the lower sampling height (4 m) the direct sea spray from the nearby coastline
251 influenced the aerosol constitution enormously. In these samples the sea-salt concentration was
252 about four to five times higher than in samples collected from the top of the tower.

253

254 □ *Please insert Table 1 here*

255

256 ***Mineral dust estimation and marine aerosol***

257 The estimation of the mineral dust content in the aerosol samples was achieved by the subtraction
258 of all determined species including the estimated mass of water, from the total mass. This was
259 done as a first approximation since major mineral dust component such as Al, Si or Fe were not
260 measured due to technical reasons. Thus, the mineral dust assumed here is analogous to the rest
261 of the undetermined aerosol component and is thus considered as the maximum possible dust
262 concentrations. The water content of the samples was estimated via the E-AIM model III of
263 Clegg et al. (Clegg et al., 1998). This model, however, delivers higher water content values than
264 the application of a hydration multiplication factor of 1.29 to the mass of all water soluble
265 inorganic compounds as suggested later (Harrison et al., 2003; Sciare et al., 2005). Using Clegg's
266 model, the average aerosol water concentration was $5.7 \pm 3.4 \mu\text{g}/\text{m}^3$. The uncertainty obtained
267 due to the application of this model was less than 10% ($0.5 \mu\text{g}/\text{m}^3$) in the estimated water content.
268 The estimated error had negligible effect on the estimated dust concentrations since the value was
269 far small compared to the uncertainty related to the determination of the other measured ions.
270 Mineral dust which in this region was mostly Saharan dust was the most dominant component of
271 the particulate matter, with a five-year average of $25.8 \pm 51.1 \mu\text{g}/\text{m}^3$ equivalent to about 55 % of
272 the total average aerosol mass concentration. Strong temporal and seasonal variations were

273 observed for the dust concentrations with concentration ranging from zero to 575.6 $\mu\text{g}/\text{m}^3$.
274 The highest dust concentration was found during the winter season due to frequent Saharan dust
275 events that were strongly influenced by the Harmattan, a characteristic wind transporting Saharan
276 dust in lower heights to the Atlantic Ocean between the end of November and the beginning of
277 March. A few heavy dust events were observed in spring and fall but not in the summer. In
278 general, differences were found in the aerosol chemical composition during days of and days
279 without dust storms.

280 The mean aerosol composition of Saharan dust dominated samples corresponding to aerosol mass
281 concentrations higher than 90 $\mu\text{g}/\text{m}^3$ and that of marine aerosol dominated days with aerosol
282 mass less than 20 $\mu\text{g}/\text{m}^3$ is shown in Figure 2. Both situations had same chemical components
283 including, water soluble ions, organic and elemental carbon, water and mineral dust, with
284 different fractional composition. As would be expected aerosol water was lower during dust
285 storms than during marine influenced days. Sea salt concentrations did not change significantly
286 during and without dust storms. However, the relative contribution of sea salt was higher in
287 marine influenced air masses than in Saharan dust air masses.

288

289 □ *Please insert Figure 2 here*

290

291 Higher concentrations were also observed for sulfate, nitrate, EC/OM, and the crustal elements
292 such as potassium and calcium during dust events as compared to marine influenced days.
293 However, their relative compositions during dust events were lower than during marine
294 influenced days due to the total absolute mass. During non-dust period long range transport from
295 the northwestern African coast, Europe and secondarily formed PM from the ocean were the
296 main sources of nss-aerosol constituents.

297 □ *Please insert Table 2 here*

298

299 **3.3 Temporal and seasonal variations**

300 Results of the measured chemical components are shown in Table 2 including their 5 year
301 averages, minima and maxima. This is the first unique dataset of nearly continuously collected
302 PM from the Cape Verde archipelago and in the region of the northern tropical Atlantic over a
303 time period of five years. In the following, the temporal and seasonal variations of the PM

304 constituents are discussed with respect to the meteorological conditions and air mass origin.
305 Figure 3 shows the time series of some of the investigated chemical components within the stated
306 time period. The red lines represent the time period during which sample collection was
307 performed on top of a container, while the blue lines represent measurements that were
308 performed on the 30 m tall tower.

309

310 □ *Please insert Figure 3 here*

311

312 **3.3.1 PM₁₀ mass concentration**

313 During the five years of PM collection at the 32 m sampling height an average mass
314 concentration of $47.1 \pm 55.5 \mu\text{g}/\text{m}^3$ was observed. Aerosol mass showed strong variability with
315 minimum and maximum values of $4.0 \mu\text{g}/\text{m}^3$ and $601.8 \mu\text{g}/\text{m}^3$, respectively (Table 2). The
316 highest and lowest daily mean concentrations were observed in January 2008 and March 2009,
317 respectively. Low concentrations were observed during days with low wind speeds of remote
318 Atlantic Ocean air mass inflow, and/or after precipitation events which typically occurred in the
319 fall. The highest aerosol mass was observed during days of Saharan dust storm when air mass
320 crossed the Saharan desert prior to their arrival at CVAO. Table 3 shows an overview of the mass
321 concentration of the number of samples sampled during different seasons. At the CVAO, particle
322 mass concentration was a good indicator for the aerosol mineral dust content. Typically, mass
323 concentrations below $20 \mu\text{g}/\text{m}^3$ were observed during marine air mass inflow (Figure 1A). When
324 aerosol mass concentrations were between $20 \mu\text{g}/\text{m}^3$ and $90 \mu\text{g}/\text{m}^3$ the air mass originated from
325 any of the three above mentioned air mass classes C to E as shown in Figures 1B-D or also of
326 marine origin with higher wind speeds. The only exception was observed when the samples were
327 collected at a 4 m height, during which sea salt concentrations increased dramatically and the
328 above mentioned features did not hold. The spikes in the PM₁₀ profile as shown in Figure 3,
329 corresponding to mass concentrations above $90 \mu\text{g}/\text{m}^3$ were indicative of days where aerosol
330 mass was dominated by Saharan dust (Figure 1B). On average, such strong Saharan dust events
331 were observed about 11-19 times a year. The duration of Saharan dust events varied from one to
332 ten days with the longest event also supported by back trajectory analysis observed from the 25th
333 of December 2007 to 4th of January 2008.

334

335 □ *Please insert Table 3 here*

336 The inter-annual variation of the monthly mean of the PM₁₀ mass concentration and seasonal
337 variation of some chemical aerosol components is shown in Figure 4. The highest mass loadings
338 were observed in 2008 and the lowest in 2009. A strong seasonal trend was found in the mass
339 loadings. The average mass concentrations were 71.8 ± 34.3 , 33.7 ± 15.3 , 36.5 ± 10.3 and $43.7 \pm$
340 $12.6 \mu\text{g}/\text{m}^3$ for winter, spring, summer and fall, respectively. The highest temporal variation was
341 observed during the winter season due to frequent change in air mass inflow. The lowest mass
342 concentrations were observed in the spring season (April to June) despite some episodic dust
343 events during this period (e.g. May 2007) while the highest concentrations were observed during
344 the late fall and winter (December to February).

345 Similar seasonal trends were reported by (Chiapello et al., 1995) for the island of Sal despite their
346 more continental location on the island whereby anthropogenic activities could strongly affect
347 mass loadings. According to (Schepanski et al., 2009) the Sahara produces larger amount of dust
348 during summer but the dust is transported at higher altitudes of up to 10 km within the Sahara Air
349 Layer while in winter the dust is transported along the north-east trade winds at far lower
350 altitudes. Thus the higher amounts of Saharan dust together with anthropogenic gaseous and
351 particulate compounds from the African continent are responsible for the winter elevated PM₁₀
352 mass concentrations while marine and non-African air mass inflow were responsible for low
353 mass loadings.

354

355 □ *Please insert Figure 4 here*

356 **3.3.2 Sea salt**

357 Sea salt concentration was estimated as $1.17 * ([\text{Na}^+] + [\text{Cl}^-])$ (Anguelova, M. D, 2002). The
358 temporal variation of sea salt concentrations is shown in Figure 3. The observed concentration of
359 sea salt was strongly dependent on the meteorological conditions and the sampling height. The
360 averaged wind speed at the CVAO was about at 7.3 m/s while the maximum wind speed
361 observed was about 13 m/s. During days with high wind speeds the sea salt concentrations
362 increased strongly. The highest wind speeds were often combined with air masses coming from
363 North America crossing the northern Atlantic to CVAO. This observation was made after the
364 back trajectory analysis and it is valid for the majority of these events.

365 During such days, the aerosol mass was slightly higher than in days with lower ($< 4 \text{ ms}^{-1}$) wind
366 speed or dominant marine air mass inflow. The averaged sea salt concentration was $11.1 \pm$

367 5.5 $\mu\text{g}/\text{m}^3$ in samples collected on top of the tower and $58.3 \pm 28.3 \mu\text{g}/\text{m}^3$ for samples collected at
368 the 4 m sampling height. Sea salt and other sea spray associated aerosol components increased
369 enormously (about a factor of 4-5) at the lower sampling height. This was due to the fact that
370 sample collection at 4 m height was done within the internal marine boundary layer (Niedermeier
371 et al. 2013) whereby aerosol mass was mostly affected by the surf zone. Increase in sea salt
372 concentrations were observed during days of high wind speeds but a strong correlation between
373 sea salt and the local wind speed was not observed. According to (de Leeuw et al., 2000) and
374 (Niedermeier et al., 2014), sea salt concentrations may increase significantly at wind speeds
375 above 10 ms^{-1} depending on the wind direction and the oceanic waves. The highest sea salt
376 concentration determined at the tower was $54 \mu\text{g}/\text{m}^3$ in spring 2011 in an episode when the local
377 wind speed was 13 ms^{-1} . The temporal variability of sea salt was not as strong as compared to
378 those of mineral dust and aerosol mass. No seasonal trend was observed in the sea salt
379 concentrations and Mg/Na ratio found in the dust (0.12) and non-dust (0.11) samples was similar
380 to the ratio in sea salt (0.12), implying no influence of the dust storms on sea salt and particularly
381 on sodium concentrations.

382

383 **3.3.3 Sulfate**

384 Sulfate consisted of sea salt sulfate (ss-sulfate) and of non-sea salt sulfate (nss-sulfate) mainly of
385 secondary origin. In Figure 3, the temporal variability of the total sulfate concentration is
386 presented. Sea salt sulfate had a similar temporal trend as sea salt, thus, the variations observed in
387 the time series are attributed to variations in nss-sulfate concentration. On the average, ss-sulfate
388 made up only 38 % of the total sulfate measured at the tower. This, however, increased when
389 sampling was done at a lower height. The highest sulfate concentrations were strongly connected
390 to Saharan dust events but not all dust events were responsible for the elevated sulfate
391 concentrations. When air mass containing dust did not have contact with anthropogenic SO_2
392 pollution sources, the nss-sulfate was not elevated and vice versa. During the dust season marine
393 sources of nss-sulfate played a minor role. The averaged nss-sulfate concentration in winter
394 marine air masses was $0.47 \pm 0.31 \mu\text{g}/\text{m}^3$ while for the dust days the averaged nss-sulfate
395 concentration was $2.46 \pm 1.05 \mu\text{g}/\text{m}^3$. The strong increase in sulfate concentrations during the
396 dust events is indicative of anthropogenic activities in Africa that influences the aerosol
397 composition. Natural sources of SO_2 are unlikely since the only nearby natural source is the
398 ocean and nss-sulfate secondary produced from oceanic precursors would therefore not vary

399 significantly with air mass origin. In Figure 4 the inter-annual and seasonal variation of nss-
400 sulfate is given. The average monthly concentration ranged from 0.43 $\mu\text{g}/\text{m}^3$ to 3.0 $\mu\text{g}/\text{m}^3$ with
401 higher concentrations observed during the summer months especially during July and August. A
402 unique source for this high summer concentration has not been identified. However, the increased
403 photochemical activity during the summer as compared to the winter months and the changes in
404 the emission of DMS due to higher biological activities in the ocean could possibly influence the
405 measured nss-sulfate concentration.

406 Elsewhere, seasonal trends have been observed for methanesulfonic acid (MSA) and DMS
407 which are known precursors of nss-sulfate with higher concentrations observed in the summer as
408 in the winter (Sciare et al., 2009). It has also been reported (Kouvarakis and Mihalopoulos, 2002;
409 Kettle et al., 1999) that sea surface water temperature influences the production of nss-sulfate and
410 other organic materials in the ocean surface micro layer leading to pronounced seasonal cycle in
411 nss-sulfate concentrations with maximum observed in summer and minimum in winter. Studies in
412 the Mediterranean sea (a region with relatively high anthropogenic pollution) have evaluated the
413 biogenic contribution to nss-sulfate concentration to be between 6 % and 22 % (Ganor et al.,
414 2000;Mihalopoulos et al., 1997). It has also been observed that under marine air mass conditions
415 the contribution of biogenic sources to nss-sulfate may rise up to 100 % (Bates et al., 1992). At
416 the CVAO, the minimum concentration of nss-sulfate during the winter and the summer was
417 about 0.20 $\mu\text{g}/\text{m}^3$ and 0.70 $\mu\text{g}/\text{m}^3$, respectively. As a first approximation, assuming that these
418 lowest concentrations of nss-sulfate were of biogenic contribution from the ocean, it would imply
419 that the biogenic contribution to the total nss-sulfate could be estimated to be averagely about 40
420 \pm 20 % in this region. Thus, although anthropogenic activities influence nss-sulfate
421 concentrations especially during dust storms and air mass coming from Europe via the Moroccan
422 coast, photochemical production of nss-sulfate and emission of marine precursors could also have
423 been important during the summer in this region.

424

425 **3.3.4 OM and EC**

426 These two carbon sum parameters showed a good correlation in their time series. The 5 year
427 average for OM and EC was 1.02 \pm 1.04 $\mu\text{g}/\text{m}^3$ and 0.13 \pm 0.16 $\mu\text{g}/\text{m}^3$, respectively. The
428 observed EC value was quite similar to the annual mean of 0.18 $\mu\text{g}/\text{m}^3$ found by Nunes et al.
429 (2013) for the year 2011 on the island of Santiago which is a slightly more anthropogenically
430 influenced region than the CVAO. Figure 3 shows the variability in both EC and OM

431 concentration over the investigated time period. Elevated EC concentrations were strongly
432 connected to elevated OM concentration but not vice versa. The number of samples with elevated
433 OM concentration was greater than those with elevated EC concentration because of additional
434 natural single sources of OM, especially during the summer. High concentrations of OM and EC
435 were strongly correlated to air masses originating from the African continent.

436 During the Harmattan season (end of November to middle of March) aerosols from the African
437 continent carried not only Saharan dust but also anthropogenic emissions from ship tracks near
438 the African coast, the African coastal cities of Dakar, Nouakchott and sometimes biomass
439 burning aerosols (EC and OM) as well as biological material into the Cape Verde region (Milton
440 et al. 2008). During such periods the EC concentration was three times higher than in air masses
441 coming from Europe and five times higher than in marine air masses. The lower transport height
442 is a further important factor for the measured elevated concentrations of dust and other aerosol
443 components during the winter season. The averaged concentration of EC and OM given in Table
444 2 were in the same range as those recently reported for marine environments (Alves et al., 2007).
445 The lowest concentration for EC was found in dominant marine air masses.

446 It has been reported that biogenic material containing organic substances of low solubility in the
447 upper sea water layer are emitted via the surface micro layer (SML) into the atmosphere and are
448 found mainly in submicron particles (O'Dowd and De Leeuw, 2007; Facchini et al., 2008; Müller
449 et al., 2009). Secondary organic aerosols formation from marine sources has also been reported in
450 different marine environment (Kawamura and Gagosian, 1987; O'Dowd et al., 2004; Facchini et
451 al., 2010). In Figure 4, the monthly and interannual variation of OM and EC are presented. A
452 strong seasonal trend is observed for OM and EC with higher values observed during the winter
453 seasons as otherwise. This winter maximum is similar to that observed for the mass concentration
454 and it is attributed to the influence of continental air masses from Africa which often carries a lot
455 of Saharan dust as well as anthropogenically emitted particles. Beside the anthropogenic sources
456 of OM and EC, OM was also be emitted from the SML of the ocean itself. The amount of the
457 marine OM production depends on oceanic biological activity which has a distinct seasonality
458 (Sciare et al., 2009). A smaller summer maximum of OM (Figure 4) was also observed which had
459 its origin from direct marine emissions or in marine emissions of gaseous precursors of PM such
460 as dimethylsulphide (DMS), isoprene, organic amines and others (Gantt et al., 2011; Gantt and
461 Meskhidze, 2013). The lowest OM concentrations were observed in April and October at CVAO.
462 With the exception of the high values observed for EC in May 2007 which was due to a dust

463 storm during this month, the EC values remain low throughout the other seasons. Thus, the high
464 EC concentration in this region was mostly due to long range transport from Africa in the dust
465 season.

466

467 **3.3.5 Nitrogen containing ions**

468 Ammonium and nitrate showed no correlation amongst each other. These ions might have had
469 other sources. The 5-year average of ammonium and nitrate were 0.09 ± 0.1 and $1.1 \pm 0.1 \mu\text{g}/\text{m}^3$,
470 respectively. (Clarke and Porter, 1993; Quinn et al., 1988) found similar ammonium
471 concentration in remote oceanic regions and suggested it could be of marine biogenic origin. The
472 concentration of both ions (ammonium and nitrate) was not influenced by the sampling height
473 implying their content in sea salt is very low. Nitrate like ammonium also showed strong
474 temporal variation (Figure 3). Ammonium concentrations varied from below detection limit to
475 $0.76 \mu\text{g}/\text{m}^3$ while nitrate concentrations varied from $0.14 \mu\text{g}/\text{m}^3$ to $3.7 \mu\text{g}/\text{m}^3$ (Table 2). This
476 strong variation was attributed to the changing air mass origin. In marine air masses the nitrate
477 concentration was lower than in air masses coming from the African or European continent
478 implying long range transport was a significant source of the observed nitrate concentrations. For
479 ammonium, summer concentrations were found to be 44 % higher than the winter concentrations
480 for clean marine air masses which would suggest that marine biological and photochemical
481 processes could strongly influence the ammonium concentrations in this region.

482 Nitrate concentrations, however, never showed a strong seasonal trend as shown on Figure 4. A
483 slight increase in the nitrate concentrations (about 20%) was often observed in the summer except
484 during 2008 where a strong decline in nitrate concentrations from January to December was
485 observed. Ammonium on the other hand, showed seasonal trends with annual maximum observed
486 in spring and early summer (Figure 4). As can be observed in Figure 4, ammonium seasonality
487 was not correlated with either the aerosol mass loading or the nss-sulfate trend. This suggests that
488 the observed ammonium in this region is not strongly linked to ammonium sulfate and may have
489 another major source different from long range transport from the continent. Marine sources of
490 NH_3 were reported earlier by Jickells et al. (2003) from isotopic measurements. Quinn et al.
491 (1988) also observed simultaneously high concentrations of ammonia in the Pacific Ocean and in
492 the oceans atmosphere and indicated that the ocean was the potential source of the ammonia.
493 They observed an averaged ammonium concentration of about $108 \text{ ng}/\text{m}^3$ in the remote north-east
494 Pacific Ocean in May which is within the same order of magnitude as that observed at CVAO

495 during May at $165 \pm 129 \text{ ng/m}^3$. Clarke and Porter (1993) have also shown good correlation
496 between atmospheric ammonium and chlorophyll A concentrations. Although long range
497 transport cannot be neglected, our results indicate that the ocean has a significant contribution to
498 the observed ammonium especially during the spring in this region.

499

500 **3.3.6 Calcium**

501 Calcium showed strong temporal variation throughout the year depending on the air mass origin
502 and sampling height (Figure 3). This variation indicates that calcium was both from sea spray and
503 mineral dust corresponding to sea salt (ss) and nss-calcium. The calcium peaks were correlated
504 with either peaks in aerosol mass loading or sea salt concentrations. The minimum and maximum
505 concentrations were $0.01 \text{ }\mu\text{g/m}^3$ and $4.44 \text{ }\mu\text{g/m}^3$, respectively. The maximum and minimum
506 values were related to days of Saharan dust events and days of dominant marine air mass inflow,
507 respectively. A strong correlation between nss-calcium and total soluble calcium (with $r^2 = 0.98$)
508 during dust events confirmed that the Saharan dust was the main source of nss-calcium in these
509 samples. Thus, soluble nss-calcium was often a good indicator for Saharan dust in this region.
510 Calcium-rich aerosol was often mobilized from NW-Sahara. During the atmospheric transport the
511 insoluble CaCO_3 was processed to more soluble compounds, e.g. in clouds. Sea salt and mineral
512 dust contributed $0.15 \pm 0.15 \text{ }\mu\text{g/m}^3$ and $0.49 \pm 0.48 \text{ }\mu\text{g/m}^3$, respectively, to the total soluble
513 calcium average concentration of $0.64 \pm 0.63 \mu\text{g/m}^3$.

514

515 **3.3.7 Potassium and Magnesium**

516 Variations in potassium and magnesium concentrations were also attributed to the varying air
517 mass inflow and the different sampling height with maximum concentrations of potassium and
518 magnesium observed at $0.86 \text{ }\mu\text{g/m}^3$ and $1.34 \text{ }\mu\text{g/m}^3$, respectively (Table 2). The 5 year average
519 concentration at the tower of potassium and magnesium were $0.13 \pm 0.09 \text{ }\mu\text{g/m}^3$ and $0.40 \pm$
520 $0.20 \text{ }\mu\text{g/m}^3$, respectively, of which nss-potassium and nss-magnesium made up only 0.02 ± 0.06
521 $\mu\text{g/m}^3$ and $0.02 \pm 0.04 \text{ }\mu\text{g/m}^3$ of the total average, respectively. This corresponds to only about 10
522 % of potassium and 5% of magnesium. Thus the ocean was the main source of these ions in this
523 region. Nss-potassium peaks were often linked with nss-calcium and mass loading peaks,
524 implying continental air masses from Africa could account for some of the nss-potassium
525 concentrations found in this region.

526 **3.3.8 Oxalate**

527 Oxalate concentrations were low in comparison to those reported in urban and continental
528 aerosols. Table 4 shows an overview of the measured oxalate concentration and those of other
529 reported works. The average oxalate concentration during polluted air masses was about $0.12 \pm$
530 $0.06 \mu\text{g}/\text{m}^3$. This value was twice as much as the concentrations observed during marine air mass
531 inflow. Comparatively to reported oxalate concentrations (Table 4), the observed concentrations
532 were within reported range. The values were higher than those reported in other marine
533 environments such as in Mace Head or Amsterdam Island (Rinaldi et al., 2011) but lower than
534 those reported in continental aerosols such as in Hong Kong (Yao et al., 2002) or Sapporo, Japan
535 (Pavuluri et al., 2012). The differences between the results in this study and the above mentioned
536 works is strongly related to the different air mass inflow regions in these areas. Mace Head is
537 more remote than CVAO while Hong Kong and Sapporo are more urban than CVAO.
538 In general, elevated oxalate concentrations were observed in polluted European and African air
539 masses (Table 4). The maximum oxalate concentration was measured at $0.46 \mu\text{g}/\text{m}^3$ in September
540 2009 during a period where air mass originated from West Africa. During the Saharan dust
541 influenced winter days, the oxalate concentration was higher than during non-dust winter days.
542 The high values were usually connected to dust storms while peaks in oxalate concentrations
543 during the summer season were connected to periods of high photochemical activity, high marine
544 activities whereby potential oxalate precursors could have been emitted to the atmosphere and
545 periods when other precursors that might have been transported from Europe. A distinct
546 seasonality in oxalate concentration was observed with a maximum during the summer season
547 (June to August). The formation of oxalate depends on the presence of organic precursors, such
548 as ethene (Warneck, 2003), glyoxal (Carlton et al., 2007), and sunlight which are more available
549 during the summer.

550

551 □ *Please insert Table 4 here*

552

553 In general, the aerosol chemical composition was influenced by sea-salt, organic compounds
554 emitted from the ocean surface micro layer, organic matter, and long range transported particulate
555 matter or precursors from anthropogenic emissions in northwestern Africa, the Canary Islands,
556 and the European continent. The Cape Verde islands themselves were only a minor source of PM
557 because of the prevailing North-East trade winds and the location of the CVAO at the
558 northeastern shore of the island São Vicente.

559

560 **3.4 Inter-relationship between ionic species**

561 **3.4.1 Nitrate and nss-sulfate**

562 Nitrate and nss-sulfate showed good correlations during the winter and the summer ($r^2 = 0.72$)
563 seasons (Nov-Apr and May-Oct, Figure 5) which could be attributed to their anthropogenic origin
564 due to observation of frequent elevation of these concentrations during long range transport from
565 Europe and Africa.

566

567 □ *Please insert Figure 5 here*

568

569 The higher slope of the regression line during summer in comparison to that of winter is
570 indicative of the presence of an additional source of nss-sulfate such as the production through
571 photochemical processes. In principle, both ions in the particle phase or their gas phase
572 precursors might be transported in higher amounts from the European and African continent
573 during winter.

574 However, during summer the photochemical production of particle phase nitrate and sulfate is
575 higher. This may therefore lead to the observed increase in the nss-sulfate concentration reflected
576 by the increase in the slope. The combined effects of increased winter emissions of anthropogenic
577 precursors reduced winter and enhanced summer photochemical conversion might explain the
578 effect depicted in Figure 5. However, further investigations are necessary in order to clearly
579 explain the difference.

580

581 **3.4.2 Nss-sulfate and Oxalate**

582 The scatter plot of nss-sulfate and oxalate shows weak correlation between both species during
583 winter and summer. However, the winter correlation (Fig. 6A) was weaker than the summer
584 correlation (Fig. 6B) with a lot of scattering in the data. These correlations were only observed
585 during days with high marine air mass influence and low aerosol mass loading with negligible
586 influence from anthropogenic emissions. During a period of eleven days with dominant marine
587 influenced air mass in spring 2011, an even stronger correlation between nss-sulfate and oxalate
588 ($r^2 = 0.90$) was observed (Fig. 6C). This suggests that there is a strong influence of surface water
589 temperatures on oxalate and nss-sulfate concentrations. It can be assumed that the clean air mass

590 was influenced by marine emissions of DMS, ethene and other marine organic precursors and
591 subsequent photochemical aqueous phase reactions might have led to the formation of oxalate
592 (Tilgner and Herrmann, 2010). As mentioned above, high surface water temperature are known
593 to also influence the production of nss-sulfate. Thus we conclude that both nss-sulfate and
594 oxalate within this period could have originated from different precursors of marine origin such
595 as from marine organisms' e.g algae or from their emissions.

596

597 □□ *Please insert Figure 6 here*

598

599 **3.4.3 Ammonium and chlorophyll A**

600 Figure 7 shows the concentration profiles of ammonium, chlorophyll A and oxalate. The
601 temporal variability of ammonium and chlorophyll A showed similar trends implying a
602 coincidence of these species. Increase in ammonium concentration was often correlated with an
603 increase in chlorophyll A concentration in the ocean's surface. The chlorophyll A concentration
604 was taken from monthly averaged MODIS Aqua satellite images over a region east and northeast
605 of São Vicente achieved from <http://disc.sci.gsfc.nasa.gov/giovanni/overview/index.html>. The
606 chlorophyll A maximum was observed between May and June. Chlorophyll A concentrations in
607 the region northeast of Cape Verde is usually higher in spring than in the other seasons and it is
608 influenced by the delivery of nutrients by higher upwelling intensity (Lathuiliere et al., 2008;
609 Ohde and Siegel, 2010) in the Mauritanian upwelling region. The observed coincidence between
610 ammonium and chlorophyll A suggest that the ocean might be a source of ammonium in this
611 region as previously illustrated above.

612

613 □ *Please insert Figure 7 here*

614

615 A similar correlation between chlorophyll A and ammonium has been reported before. (Clarke
616 and Porter, 1993) found a good correlation between enhanced ammonium aerosol concentrations
617 and enhanced chlorophyll concentrations during an equatorial Pacific Ocean cruise and
618 concluded that the observed ammonia was a result of equatorial upwelling. (Jickells et al., 2003)
619 also concluded on the basis of isotopic measurements of ammonium in marine aerosols that the
620 ocean was a possible source of their observed ammonium concentrations in the North and South
621 Atlantic Ocean.

622 (Quinn et al., 1988) also observed ammonia in the remote Pacific Ocean and the atmosphere and
623 concluded that the observed atmospheric ammonium originated from the ocean. Although the
624 ocean is a significant source of ammonia during remote conditions, long range transport of
625 ammonia or ammonium salts from the African continent or SW Europe were also important
626 sources of ammonia in this region.

627

628 **3.4.4 Elemental carbon (EC) and nss-potassium**

629 A similar temporal variation was observed in the time series of nss-potassium and elemental
630 carbon concentrations during dust events when elevated OC and EC concentrations were
631 observed (Figure 8) with correlation factor ($r^2 = 0.6$). In principle, this correlation was only
632 observed during about 50% of the time when air mass inflow was from Africa. Nss-potassium is
633 a known tracer for biomass burning activities. This correlation thereby suggests that biomass
634 burning could partly account for the observed EC concentrations at CVAO especially during air
635 mass inflow from Africa. However, when the air mass origin was from Europe or from the
636 oceans, no correlation could be observed between nss-potassium and EC.

637

638 □ *Please insert Figure 8 here*

639

640 **3.5 Bromide and chloride depletion in PM₁₀**

641 Bromide and chloride deficits indicate significant reactive cycling of halogens and do influence
642 the reactive capacity of the marine environment by release of more reactive chloride to the
643 atmosphere. Bromide and chloride deficits in marine aerosols have been reported in different
644 marine environments (Mozurkewich, 1995; Kerminen et al., 1998; Kumar and Sarin, 2010; Yao
645 and Zhang, 2012). The reported (Liebezeit, 2011) sodium to chloride (bromide) mass ratio in sea-
646 salt is 0.56 (162.4), and the molar ratio is 0.85 (46.73). The chloride (bromide) depletion is
647 estimated as the percentage loss in chloride (bromide) from sea salt chloride (bromide)
648 concentrations leading to higher values of the sodium to chloride (bromide) ratios. In the
649 atmosphere, when bromide and chloride react with acidic gases or particles containing nitric,
650 sulfuric, or organic acids to form HOX, X₂ and other compounds, the evaporation of volatile
651 bromine/chlorine compounds occur and bromide and chloride losses are observed in marine
652 aerosols leading to an increase in the sodium to chloride (bromide) ratio. This effect of

653 bromide/chloride depletion is known to increase with decreasing particle size from about 30 % to
654 100 % in the presence of anthropogenic pollutants (Hsu et al., 2007; Quinn and Bates, 2005). In
655 this study, bromide and chloride depletion was observed in PM₁₀ samples and are discussed
656 according to seasons, sampling height and dust concentration.

657

658 □ *Please insert Figure 9 here*

659 □ *Please insert Table 5 here*

660

661 Figure 9 shows the temporal variation in the chloride/bromide depletion and aerosol mass
662 concentration during 5 years of measurements at CVAO. Bromide loss was always higher than
663 chloride loss with average bromide and chloride losses of about 80 % and 16 %, respectively.
664 Periods of Saharan dust influence observed as peaks in the aerosol mass concentrations usually
665 yielded 62 % bromide and 9 % chloride loss.

666 At lower sampling height, fresh sea spray particles have shorter residence time in the atmosphere
667 prior to their collection and thus should have insignificant bromide/chloride deficits. However,
668 due to the mixture of aged and long range transported aerosols with the freshly emitted marine
669 particles, bromide (chloride) depletion of about 4 % was observed at this height. In Table 5 the
670 average chloride and bromide deficits for the typical air mass inflow of the particles and their
671 precursors are given. Higher halogen depletion was observed during periods of low aerosol mass
672 concentration with less influence of Saharan dust. Long range transported and aged sea-salt
673 particles loose more chloride (bromide) due to their long atmospheric residence time and thus
674 more time for interaction with acidic compounds. The highest chloride (bromide) loss of about
675 30% (87 %) was observed when air mass crossed southwest Europe prior to its arrival at CVAO
676 and had relatively long (72 h) residence time over the ocean. The more anthropogenically
677 influenced SW European particles and gaseous compounds thus had sufficient time to adsorb
678 onto and react with sea salt particles resulting in a higher exchange and displacement of
679 halogenides from sea salt particles as compared to periods when particles spends less time over
680 the ocean as it's the case during Saharan dust events.

681 The chloride depletion during winter and summer marine air masses (Figure 1A), was about 5%
682 lower than the loss observed during SW Europe influenced air mass inflow. The air mass origin,
683 aerosol acidic component concentration and the sea salt particle atmospheric life time were the
684 determining factors towards the halogenide depletion. The deficits were higher in the summer

685 than in the winter. This was likely due to varying solar irradiation intensity and the concentration
686 difference of the aerosol acidic components of sulfuric and nitric acid in these samples. During
687 marine influenced air mass inflow the nss-sulfate concentration in the summer was twice as much
688 as that observed in the winter, likely due to the increase in photochemical production activities
689 and the emission of marine nss-sulfate precursors as previously explained. Thus the additional
690 nss-sulfate source and higher solar irradiation are most probably one of the reasons for the
691 increased chloride/bromide loss during the summer in comparison to the winter for marine
692 influenced air masses.

693 Nevertheless, although the concentration of nitrate and non-sea salt sulfate was high during
694 Saharan dust events, the chloride/bromide depletion was found to be the lowest. Figure 9 depicts
695 a clear anti-correlation between PM mass concentration and halogenide loss. This effect was
696 clearly seen in winter 2007/08 and 2010/11. During the winter 2008/09 the dust events were less
697 intensive and the winter sampling period 2009/10 took place at a lower sampling height with a
698 greater influence of sea spray.

699 During dust events there is not only an increase in acidic species, but also an increase in cations
700 and carbonates. The increase in cations concentration provides additional reactive sites for the
701 acidic species thus reducing the possibility for the direct reaction on sea salt particles, and
702 therefore, decreasing the overall displacement of halogenides from sodium. Furthermore, gaseous
703 halogenides could react with CaCO_3 as shown by (Sullivan et al., 2007) leading to a buffering
704 effect of the dust on the sea salt particles thereby resulting in a more externally mixed aerosol.
705 Thus a combination of low residence time as mentioned above and higher competition of cations
706 sites during dust events leads to a lower effective loss of chloride and bromide from sea salt
707 particles in comparison to the other situations. We thus suggest that in this region of the Atlantic,
708 these three processes, photochemistry, air mass residence time and concentration of acidic
709 components are the determining driving factors towards halogenide deficits in the observed
710 aerosol.

711

712 **3.5.1 Contribution of acidic species to chloride depletion**

713 The most important aerosol acidic species are nitric and sulfuric acids since their concentrations
714 are far higher than those of other acidic species such as oxalic acid (in non-dusty aerosol). As
715 explained above, the highest chloride deficit was observed when air mass inflow was from
716 Europe. The scatter plot of equivalent concentrations of Na^+ and Cl^- (Figure 10A) shows that the

717 data points fall below the theoretical values in sea water and only approaches this line when the
718 Cl^- concentration is matched with nitrate and nss-sulfate concentrations (Figure 10B). Thus,
719 assuming all available nitrate and nss-sulfate species were involved in chloride depletion, this
720 would account only for about 90% of the chloride depletion. The actual contribution of these
721 species is, however, much less since they may also be associated with NH_4^+ , nss-K^+ or Ca^{2+} that
722 are possible neutralizers of the available nitric and sulfuric acids. Thus, considering the
723 neutralization of sulfuric or nitric acid by ammonium or other cations, the excess sulfuric or nitric
724 acid available will be even less and they would thus account for less than 90% of the chloride
725 depletion. This indicates that during air mass inflow from Europe other process mechanisms
726 different from acid displacement reactions such as photochemical reactions with ozone or NO
727 (Behnke and Zetzsch, 1990) could have been involved in chloride depletion.

728

729 □ *Please insert Figure 10 here*

730

731 A similar tendency was observed in samples where air mass inflow was of marine origin during
732 the summer. The estimated chloride loss was about 26 % and the concentrations of the acidic
733 components were also elevated, but the acid displacement of neither nitric nor sulfuric acids was
734 sufficient to account for the chloride loss. Their contribution however could only explain about
735 95 % of the chloride loss assuming these species were not associated with other cations. The only
736 situation whereby acidic species could sufficiently account for chloride loss was during Saharan
737 dust events as shown in Figure 10C and 10D. The scatter plot shows good correlation slightly
738 above theoretical sea water line for Na^+ and Cl^- when Cl^- concentrations are marched with NO_3^- ,
739 indicating that, within error margins, nitric acid displacement was the main reaction leading to
740 chloride loss while during dust events. This claim is supported by results of size resolved
741 distribution of aerosol components previously reported by (Müller et al., 2010) which showed
742 that during dust events, about 90 % of nitrate is found in the coarse mode together with sea salt
743 particles while nss-sulfate concentration are concentrated in the fine mode. Thus in all non-
744 Saharan dust influenced days at CVAO, photochemistry was a determining factor towards
745 chloride loss while during dust events, nitric acid played the major role.

746

747

748 3.6 PMF source apportionment analysis

749 The positive matrix factorization analysis (PMF) was applied to identify the possible sources of
750 the aerosol observed at the CVAO during the investigated time period. The chemical composition
751 matrix was made of the 12 analyzed chemical species (water soluble ions, OC and EC). Three
752 major sources were identified by having clear different signatures as fresh sea-salt, aged sea-salt
753 and long range transport. Figure 11 shows the source profiles (blue bars) and the relative
754 contribution of each factor to the total species concentration in the samples (red squares). There
755 was no ideal tracer for mineral dust since trace metal analysis were not performed on these filters.
756 However, due to the strong correlation between $nss-Ca^{2+}$ and Ca^{2+} during dust storms ($r^2 = 0.99$),
757 calcium occurrence was considered as a possible indicator of mineral dust or long range
758 transported dust particles. The fresh sea salt factor was characterized by similar (Liebezeit, 2011)
759 sea water proportions of Na (35 %), Cl (54 %), sulfate (7 %) and magnesium (4 %). The model
760 obtained fractions were quite similar to reported sea water concentration and indicated that PMF
761 is a useful tool in identifying sources in complex aerosol samples. In principle, this factor
762 represents freshly emitted sea salt particles due the strong agreement with sea water proportions
763 and the little association with non-sea salt species. Thus, freshly emitted sea salt particles
764 dominated the ionic composition of the aerosol as it made up about 50 % of its ionic and organic
765 matter content (Figure 12). This factor could account for the total bromide and 50 % of chloride,
766 sodium, potassium and magnesium concentrations in the samples.

767

768 □ *Please insert Figure 11 and Figure 12 here*

769

770 The aged sea salt source was the second most important source making up about 36% of the total
771 ionic and organic mass. It was characterized by elevated sulfate (14 %), nitrate (6 %) and OC
772 (4 %) concentrations associated with sea salt particles. This source describes sea salt particles that
773 interact with acidic gases or marine emitted organic matter such as SOA and nss-sulfate from
774 DMS chemistry. The lower chloride (42 %) to sodium (31 %) ratio in this factor is a strong
775 indication of chloride loss due to one of the processes mentioned above. As has also been
776 reported in other works (Amato et al., 2009), sulfate and nitrate association with sea salt particles
777 in this work was also considered as an indicator for the aged sea salt source. This source could
778 account for about 62 % of the total observed soluble calcium, 58 % of the sulfate, 45 % of the

779 nitrate and 25 % of the organic matter observed in the samples.
780 Finally, the long range transport factor was characterized by calcium, organic and elemental
781 carbon, as well as elevated sulfate and nitrate concentrations. This factor could explain 14% of
782 the source of the investigated ionic and organic components. The unique tracer for this factor was
783 the presence of EC. EC as well as OC can originate from traffic emissions, biomass burning, or
784 ship emissions. Emitted particles from such anthropogenic activities may only reach the CVAO
785 via long range transport. This factor could account for the presence of all EC, 80% of the OC and
786 60% of the nitrate observed at the CVAO. A comparison of this factor with our Saharan dust
787 estimation showed most of the time a similar time series. Therefore, the estimated mineral dust
788 profile could be explained by the long range transport source.
789 Although the PMF model could not successfully separate mineral dust and long range transported
790 particles due to the limited data input, the obtained results are still representative of this region of
791 the Atlantic and are unique and show that mineral dust contributes to not more than 14 % of the
792 water soluble ions and organic mass budget at CVAO.

793

794 **4. Conclusions**

795 Saharan dust and sea salt dominate the PM₁₀ particle composition in near surface air masses at
796 the CVAO. At the standard collection height of 32 m at the CVAO, the long term mean of sea
797 salt and total PM₁₀ aerosol were 11 µg/m³ and 47 µg/m³, respectively, of which Saharan dust
798 made up 55% of the PM₁₀ mass. Secondary ionic species, elemental carbon, organic matter and
799 water completed the particle composition. Seasonal variations were found for aerosol mass, dust,
800 nss-sulfate, EC, OM and ammonium. Ammonium and oxalate were often correlated with
801 chlorophyll A which suggests that ammonia and oxalic acid had also marine precursors in this
802 environment. A distinct seasonality was observed for the halogenide depletion with the minimum
803 in winter due to the occurrence of Saharan dust events and the lower irradiation intensity in non-
804 dust periods. Chloride depletion varied between 10 % and 35 %. In marine air masses during the
805 summer and in polluted air masses from SW Europe, bromide was often fully depleted while
806 chloride observed its highest depletions. Photochemistry, air mass residence time and
807 concentration of acidic components were the main factors controlling halogenide depletion in this
808 region. While photochemistry was decisive during summer, nitric acid played a major role
809 towards chloride depletion during dust storms.

810 Ground based long-term investigation of PM at the CVAO is an important step towards
811 understanding the role of aerosols in ocean atmosphere interactions especially in the tropical
812 Northeast Atlantic. The observed strong annual and seasonal variation of the aerosol constitution
813 provides useful information to the type of atmospheric nutrient deposition and the ocean responds
814 to this deposition over the past five years. Such investigations are quite useful since they provide
815 the relevant background knowledge for understanding in the long term the role the atmosphere
816 and the Ocean plays in the global climate. Such long term observations are highly encouraged
817 and would be essential in initializing model runs that can then in more detail describe the link
818 between the atmosphere ocean interaction and the global climate. Air mass origins with dust
819 source regions, oceanic and meteorological influences during air mass transport must be further
820 investigated to understand their effects on the global climate.

821

822 **Acknowledgements**

823 The efforts of Luis Mendes and Helder Timas Nascimento for sampling and maintenance
824 activities at the CVAO and of the TROPOS laboratory assistants for their helpful work are
825 greatly appreciated. The study was supported by the German BMBF within the SOPRAN I and II
826 projects (FKZ: 03F0462J and 03F0611J) and the EU specific Support Action TENATSO
827 (37090).

828

829

830

831

832

833

834

835

836

837

838

839

840

841 **5.0 References**

- 842 Alastuey, A., Querol, X., Castillo, S., Escudero, M., Avila, A., Cuevas, E., Torres, C., Romero, P.
843 M., Exposito, F., Garcia, O., Diaz, J. P., Van Dingenen, R., and Putaud, J. P.: Characterisation of
844 TSP and PM_{2.5} at Izana and Sta. Cruz de Tenerife (Canary Islands, Spain) during a Saharan dust
845 episode (July 2002), *Atmos Environ*, 39, 4715-4728, DOI 10.1016/j.atmosenv.2005.04.018,
846 2005.
- 847 Allan, J. D., Topping, D. O., Good, N., Irwin, M., Flynn, M., Williams, P. I., Coe, H., Baker, A.
848 R., Martino, M., Niedermeier, N., Wiedensohler, A., Lehmann, S., Müller, K., Herrmann, H., and
849 McFiggans, G.: Composition and properties of atmospheric particles in the eastern Atlantic and
850 impacts on gas phase uptake rates, *Atmos Chem Phys*, 9, 9299-9314, 2009.
- 851 Alves, C., Oliveira, T., Pio, C., Silvestre, A. J. D., Fialho, P., Barata, F., and Legrand, M.:
852 Characterisation of carbonaceous aerosols from the Azorean Island of Terceira, *Atmos Environ*,
853 41, 1359-1373, DOI 10.1016/j.atmosenv.2006.10.022, 2007.
- 854 Amato, F., Pandolfi, M., Escrig, A., Querol, X., Alastuey, A., Pey, J., Perez, N., and Hopke, P.
855 K.: Quantifying road dust resuspension in urban environment by Multilinear Engine: A
856 comparison with PMF₂, *Atmos Environ*, 43, 2770-2780, DOI 10.1016/j.atmosenv.2009.02.039,
857 2009.
- 858 Anguelova, M. D, Whitecaps, sea-salt aerosols, and climate, Ph.D. Dissertation, University of
859 Delaware, 2002.
- 860 Bates, T. S., Lamb, B. K., Guenther, A., Dignon, J., and Stoiber, R. E.: Sulfur emissions to the
861 atmosphere from natural sources, *J Atmos Chem*, 14, 315-337, 1992.
- 862 Bates, T. S., Quinn, P. K., Coffman, D. J., Johnson, J. E., Miller, T. L., Covert, D. S.,
863 Wiedensohler, A., Leinert, S., Nowak, A., and Neusüss, C.: Regional physical and chemical
864 properties of the marine boundary layer aerosol across the Atlantic during Aerosols99: An
865 overview, *J Geophys Res-Atmos*, 106, 20767-20782, 2001.
- 866 Behnke, W., and Zetzsch, C.: Heterogeneous photochemical formation of Cl-atoms from NaCl
867 aerosol, NO_x and ozone, *J Aerosol Sci*, 21, S229-S232, Doi 10.1016/0021-8502(90)90226-N,
868 1990.
- 869 Canonaco, F., Crippa, M., Slowik, J. G., Prévôt, A. S. H., and Baltensperger, U.: SoFi, an Igor
870 based interface for the efficient use of the generalized Multilinear Engine (ME-2) for source
871 apportionment: application to aerosol mass spectrometer data, *Atmos. Meas. Tech. Discuss.*, 6,
872 6409 - 6443, doi: 10.5194/amtd-6-6409-2013, 2013.
- 873 Carlton, A. G., Turpin, B. J., Altieri, K. E., Seitzinger, S., Reff, A., Lim, H. J., and Ervens, B.:
874 Atmospheric oxalic acid and SOA production from glyoxal: Results of aqueous photooxidation
875 experiments, *Atmos Environ*, 41, 7588-7602, DOI 10.1016/j.atmosenv.2007.05.035, 2007.
- 876 Carpenter, E. J., Subramaniam, A., and Capone, D. G.: Biomass and primary productivity of the
877 cyanobacterium *Trichodesmium* spp. in the tropical N Atlantic ocean, *Deep-Sea Res Pt I*, 51,
878 173-203, DOI 10.1016/j.dsr.2003.10.006, 2004.
- 879 Carpenter, L. J., Fleming, Z. L., Read, K. A., Lee, J. D., Moller, S. J., Hopkins, J. R., Purvis, R.
880 M., Lewis, A. C., Müller, K., Heinold, B., Herrmann, H., Fomba, K. W., van Pinxteren, D.,
881 Muller, C., Tegen, I., Wiedensohler, A., Müller, T., Niedermeier, N., Achterberg, E. P., Patey, M.
882 D., Kozlova, E. A., Heimann, M., Heard, D. E., Plane, J. M. C., Mahajan, A., Oetjen, H., Ingham,
883 T., Stone, D., Whalley, L. K., Evans, M. J., Pilling, M. J., Leigh, R. J., Monks, P. S.,
884 Karunaharan, A., Vaughan, S., Arnold, S. R., Tschritter, J., Pohler, D., Friess, U., Holla, R.,
885 Mendes, L. M., Lopez, H., Faria, B., Manning, A. J., and Wallace, D. W. R.: Seasonal
886 characteristics of tropical marine boundary layer air measured at the Cape Verde Atmospheric

887 Observatory, *J Atmos Chem*, 67, 87-140, DOI 10.1007/s10874-011-9206-1, 2010.

888 Chen, Y., and Siefert, R. L.: Determination of various types of labile atmospheric iron over
889 remote oceans, *J Geophys Res-Atmos*, 108, Artn 4774 Doi 10.1029/2003jd003515, 2003.

890 Chen, Y., and Siefert, R. L.: Seasonal and spatial distributions and dry deposition fluxes of
891 atmospheric total and labile iron over the tropical and subtropical North Atlantic Ocean, *J*
892 *Geophys Res-Atmos*, 109, Artn D09305 Doi 10.1029/2003jd003958, 2004.

893 Chiapello, I., Bergametti, G., Gomes, L., Chatenet, B., Dulac, F., Pimenta, J., and Soares, E. S.:
894 An additional low layer transport of Sahelian and Saharan dust over the north-eastern tropical
895 Atlantic, *Geophys Res Lett*, 22, 3191-3194, Doi 10.1029/95gl03313, 1995.

896 Chiapello, I., Prospero, J. M., Herman, J. R., and Hsu, N. C.: Detection of mineral dust over the
897 North Atlantic Ocean and Africa with the Nimbus 7 TOMS, *J Geophys Res-Atmos*, 104, 9277-
898 9291, 1999.

899 Clarke, A. D., and Porter, J. N.: Pacific marine aerosol .2. Equatorial gradients in chlorophyll,
900 ammonium, and excess sulfate during Saga-3, *J Geophys Res-Atmos*, 98, 16997-17010, 1993.

901 Clegg, S. L., Brimblecombe, P., and Wexler, A. S.: Thermodynamic model of the system H^+ -
902 NH_4^+ - Na^+ - SO_4^{2-} - NH_3 - Cl^- - H_2O at 298.15 K, *J Phys Chem A*, 102, 2155-2171, Doi
903 10.1021/Jp973043j, 1998.

904 Cropp, R. A., Gabric, A. J., McTainsh, G. H., Braddock, R. D., and Tindale, N.: Coupling
905 between ocean biota and atmospheric aerosols: Dust, dimethylsulphide, or artifact?, *Global*
906 *Biogeochem Cy*, 19, Artn Gb4002 Doi 10.1029/2004gb002436, 2005.

907 De Leeuw, G., Neele, F. P., Hill, M., Smith, M. H., and Vignali, E.: Production of sea spray
908 aerosol in the surf zone, *J Geophys Res-Atmos*, 105, 29397-29409, Doi 10.1029/2000jd900549,
909 2000.

910 Facchini, M. C., Decesari, S., Rinaldi, M., Carbone, C., Finessi, E., Mircea, M., Fuzzi, S.,
911 Moretti, F., Tagliavini, E., Ceburnis, D., and O'Dowd, C. D.: Important source of marine
912 secondary organic aerosol from biogenic amines, *Environ Sci Technol*, 42, 9116-9121, Doi
913 10.1021/Es8018385, 2008.

914 Facchini, M. C., Decesari, S., Rinaldi, M., Finessi, E., Ceburnis, D., O'Dowd, C. D., and
915 Stephanou, E. G.: Marine SOA: Gas-to-particle conversion and oxidation of primary organic
916 aerosol, *Geochim Cosmochim Acta*, 74, A275-A275, 2010.

917 Fomba, K. W., Müller, K., van Pinxteren, D., and Herrmann, H.: Aerosol size-resolved trace
918 metal composition in remote northern tropical Atlantic marine environment: case study Cape
919 Verde islands, *Atmos Chem Phys*, 13, 4801-4814, DOI 10.5194/acp-13-4801-2013, 2013.

920 Formenti, P., Elbert, W., Maenhaut, W., Haywood, J., and Andreae, M. O.: Chemical
921 composition of mineral dust aerosol during the Saharan Dust Experiment (SHADE) airborne
922 campaign in the Cape Verde region, September 2000, *J Geophys Res-Atmos*, 108, Artn 8576
923 Doi 10.1029/2002jd002648, 2003.

924 Formenti, P., Schutz, L., Balkanski, Y., Desboeufs, K., Ebert, M., Kandler, K., Petzold, A.,
925 Scheuvsens, D., Weinbruch, S., and Zhang, D.: Recent progress in understanding physical and
926 chemical properties of African and Asian mineral dust, *Atmos Chem Phys*, 11, 8231-8256, DOI
927 10.5194/acp-11-8231-2011, 2011.

928 Ganor, E., Foner, H. A., Bingemer, H. G., Udusti, R., and Setter, I.: Biogenic sulphate generation
929 in the Mediterranean Sea and its contribution to the sulphate anomaly in the aerosol over Israel
930 and the Eastern Mediterranean, *Atmos Environ*, 34, 3453-3462, 2000.

931 Gantt, B., Meskhidze, N., Facchini, M. C., Rinaldi, M., Ceburnis, D., and O'Dowd, C. D.: Wind
932 speed dependent size-resolved parameterization for the organic mass fraction of sea spray
933 aerosol, *Atmos Chem Phys*, 11, 8777-8790, DOI 10.5194/acp-11-8777-2011, 2011.

934 Gantt, B., and Meskhidze, N.: The physical and chemical characteristics of marine primary
935 organic aerosol: a review, *Atmos Chem Phys*, 13, 3979-3996, DOI 10.5194/acp-13-3979-2013,
936 2013.

937 Gelado-Caballero, M. D., Lopez-Garcia, P., Prieto, S., Patey, M. D., Collado, C., and Hernandez-
938 Brito, J. J.: Long-term aerosol measurements in Gran Canaria, Canary Islands: Particle
939 concentration, sources and elemental composition, *J Geophys Res-Atmos*, 117, Artn D03304
940 Doi 10.1029/2011jd016646, 2012.

941 Gnauk, T., Muller, K., van Pinxteren, D., He, L. Y., Niu, Y. W., Hu, M., and Herrmann, H.: Size-
942 segregated particulate chemical composition in Xinken, Pearl River Delta, China: OC/EC and
943 organic compounds, *Atmos Environ*, 42, 6296-6309, DOI 10.1016/j.atmosenv.2008.05.001,
944 2008.

945 Harrison, R. M., Jones, A. M., and Lawrence, R. G.: A pragmatic mass closure model for
946 airborne particulate matter at urban background and roadside sites, *Atmos Environ*, 37, 4927-
947 4933, DOI 10.1016/j.atmosenv.2003.08.025, 2003.

948 Heller, M. I., and Croot, P. L.: Superoxide decay as a probe for speciation changes during dust
949 dissolution in Tropical Atlantic surface waters near Cape Verde, *Mar Chem*, 126, 37-55, DOI
950 10.1016/j.marchem.2011.03.006, 2011.

951 Hsu, S. C., Liu, S. C., Kao, S. J., Jeng, W. L., Huang, Y. T., Tseng, C. M., Tsai, F., Tu, J. Y., and
952 Yang, Y.: Water-soluble species in the marine aerosol from the northern South China Sea: High
953 chloride depletion related to air pollution, *J Geophys Res-Atmos*, 112, Artn D19304
954 Doi 10.1029/2007jd008844, 2007.

955 Jaenicke, R.: Atmospheric aerosols and global climate, *J Aerosol Sci*, 11, 577-588, Doi
956 10.1016/0021-8502(80)90131-7, 1980.

957 Jickells, T. D., Kelly, S. D., Baker, A. R., Biswas, K., Dennis, P. F., Spokes, L. J., Witt, M., and
958 Yeatman, S. G.: Isotopic evidence for a marine ammonia source, *Geophys Res Lett*, 30, Artn
959 1374 Doi 10.1029/2002gl016728, 2003.

960 Johansen, A. M., Siefert, R. L., and Hoffmann, M. R.: Chemical composition of aerosols
961 collected over the tropical North Atlantic Ocean, *J Geophys Res-Atmos*, 105, 15277-15312, Doi
962 10.1029/2000jd900024, 2000.

963 Kandler, K., Benker, N., Bundke, U., Cuevas, E., Ebert, M., Knippertz, P., Rodriguez, S., Schutz,
964 L., and Weinbruch, S.: Chemical composition and complex refractive index of Saharan mineral
965 dust at Izana, Tenerife (Spain) derived by electron microscopy, *Atmos Environ*, 41, 8058-8074,
966 DOI 10.1016/j.atmosenv.2007.06.047, 2007.

967 Kandler, K., Lieke, K., Benker, N., Emmel, C., Kupper, M., Muller-Ebert, D., Ebert, M.,
968 Scheuvsens, D., Schladitz, A., Schutz, L., Weinbruch, S.: Electron microscopy of particles
969 collected at Praia, Cape Verde, during the Saharan Mineral Dust Experiment: particle chemistry,
970 shape, mixing state and complex refractive index. *Tellus B* 63, 475-496, 2011.

971 Kawamura, K., and Gagosian, R. B.: Implications of omega-oxocarboxylic acids in the remote
972 marine atmosphere for photooxidation of unsaturated fatty-acids, *Nature*, 325, 330-332, 1987.

973 Kawamura, K., and Sakaguchi, F.: Molecular distributions of water soluble dicarboxylic acids in
974 marine aerosols over the Pacific Ocean including tropics, *J Geophys Res-Atmos*, 104, 3501-3509,
975 Doi 10.1029/1998jd100041, 1999.

976 Kelly, J. T., Chuang, C. C., and Wexler, A. S.: Influence of dust composition on cloud droplet
977 formation, *Atmos Environ*, 41, 2904-2916, DOI 10.1016/j.atmosenv.2006.12.008, 2007.

978 Kerminen, V. M., Teinila, K., Hillamo, R., and Pakkanen, T.: Substitution of chloride in sea-salt
979 particles by inorganic and organic anions, *J Aerosol Sci*, 29, 929-942, 1998.

980 Kettle, A. J., Andreae, M. O., Amouroux, D., Andreae, T. W., Bates, T. S., Berresheim, H.,

981 Bingemer, H., Boniforti, R., Curran, M. A. J., DiTullio, G. R., Helas, G., Jones, G. B., Keller, M.
982 D., Kiene, R. P., Leck, C., Lévasseur, M., Malin, G., Maspero, M., Matrai, P., McTaggart, A. R.,
983 Mihalopoulos, N., Nguyen, B. C., Novo, A., Putaud, J. P., Rapsomanikis, S., Roberts, G.,
984 Schebeske, G., Sharma, S., Simo, R., Staubes, R., Turner, S., and Uher, G.: A global database of
985 sea surface dimethylsulfide (DMS) measurements and a procedure to predict sea surface DMS as
986 a function of latitude, longitude, and month, *Global Biogeochem Cy*, 13, 399-444, 1999.

987 Kouvarakis, G., and Mihalopoulos, N.: Seasonal variation of dimethylsulfide in the gas phase and
988 of methanesulfonate and non-sea-salt sulfate in the aerosols phase in the Eastern Mediterranean
989 atmosphere, *Atmos Environ*, 36, 929-938, 2002.

990 Kumar, A., and Sarin, M. M.: Atmospheric water-soluble constituents in fine and coarse mode
991 aerosols from high-altitude site in western India: Long-range transport and seasonal variability,
992 *Atmos Environ*, 44, 1245-1254, DOI 10.1016/j.atmosenv.2009.12.035, 2010.

993 Lathuiliere, C., Echevin, V., and Levy, M.: Seasonal and intraseasonal surface chlorophyll-a
994 variability along the northwest African coast, *J Geophys Res-Oceans*, 113, Artn C05007
995 Doi 10.1029/2007jc004433, 2008.

996 Lee, J.D., McFiggans, G., Allan, J.D., Baker, A.R., Ball, S.M., Benton, A.K., Carpenter, L.J.,
997 Commane, R., Finley, B.D., Evans, M., Fuentes, E., Furneaux, K., Goddard, A., Good, N.,
998 Hamilton, J.F., Heard, D.E., Herrmann, H., Hollingsworth, A., Hopkins, J.R., Ingham, T., Irwin,
999 M., Jones, C.E., Jones, R.L., Keene, W.C., Lawler, M.J., Lehmann, S., Lewis, A.C., Long, M.S.,
1000 Mahajan, A., Methven, J., Moller, S.J., Müller, K., Müller, T., Niedermeier, N., O'Doherty, S.,
1001 Oetjen, H., Plane, J.M.C., Pszenny, A.A.P., Read, K.A., Saiz-Lopez, A., Saltzman, E.S., Sander,
1002 R., von Glasow, R., Whalley, L., Wiedensohler, A., Young, D.: Reactive halogens in the marine
1003 boundary layer (RHaMBLe): the tropical North Atlantic experiments. *Atmos. Chem. Phys.* 10,
1004 1031-1055, 2010.

1005 G.Liebezeit, Meereschemie und globaler Wandel. In: Warnsignal Klima - Die Meere -
1006 Änderungen & Risiken. Eds. J.L. Lozán, H. Graßl, L. Karbe, K. Reise, Wissenschaftliche
1007 Auswertungen, Hamburg, p. 32, 2011.

1008 Mahajan, A. S., Plane, J. M. C., Oetjen, H., Mendes, L., Saunders, R. W., Saiz-Lopez, A., Jones,
1009 C. E., Carpenter, L. J., and McFiggans, G. B.: Measurement and modelling of tropospheric
1010 reactive halogen species over the tropical Atlantic Ocean, *Atmos Chem Phys*, 10, 4611-4624,
1011 DOI 10.5194/acp-10-4611-2010, 2010.

1012 Mahowald, N. M., Baker, A. R., Bergametti, G., Brooks, N., Duce, R. A., Jickells, T. D.,
1013 Kubilay, N., Prospero, J. M., and Tegen, I.: Atmospheric global dust cycle and iron inputs to the
1014 ocean, *Global Biogeochem Cy*, 19, Artn Gb4025 Doi 10.1029/2004gb002402, 2005.

1015 Mihalopoulos, N., Stephanou, E., Kanakidou, M., Pilitsidis, S., and Bousquet, P.: Tropospheric
1016 aerosol ionic composition in the Eastern Mediterranean region, *Tellus B*, 49, 314-326, 1997.

1017 Milton, S.F., Greed, G., Brooks, M.E., Haywood, J., Johnson, B., Allan, R.P., Slingo, A., Grey,
1018 W.M.F.: Modeled and observed atmospheric radiation balance during the West African dry
1019 season: Role of mineral dust, biomass burning aerosol, and surface albedo. *J. Geophys. Res.-*
1020 *Atmos.* 113, 2008.

1021 Mozurkewich, M.: Mechanisms for the release of halogens from sea-salt particles by free-radical
1022 reactions, *J Geophys Res-Atmos*, 100, 14199-14207, Doi 10.1029/94jd00358, 1995.

1023 Müller, C., Inuma, Y., Karstensen, J., van Pinxteren, D., Lehmann, S., Gnauk, T., and Herrmann,
1024 H.: Seasonal variation of aliphatic amines in marine sub-micrometer particles at the Cape Verde
1025 islands, *Atmos Chem Phys*, 9, 9587-9597, 2009.

1026 Müller, K., Lehmann, S., van Pinxteren, D., Gnauk, T., Niedermeier, N., Wiedensohler, A., and
1027 Herrmann, H.: Particle characterization at the Cape Verde atmospheric observatory during the

1028 2007 RHaMBLe intensive, *Atmos Chem Phys*, 10, 2709-2721, 2010.

1029 Neusüss, C., Wex, H., Birmili, W., Wiedensohler, A., Koziar, C., Busch, B., Brüggemann, E.,
1030 Gnauk, T., Ebert, M., and Covert, D. S.: Characterization and parameterization of atmospheric
1031 particle number-, mass-, and chemical-size distributions in central Europe during LACE 98 and
1032 MINT, *J Geophys Res-Atmos*, 107, Artn 8127 Doi 10.1029/2001jd000514, 2002.

1033 Niedermeier, N., Held, A., Müller, T., Heinold, B., Schepanski, K., Tegen, I., Kandler, K., Ebert,
1034 M., Weinbruch, S., Read, K., Lee, J., Fomba, K. W., Müller, K., Herrmann, H., and
1035 Wiedensohler, A.: Mass deposition fluxes of Saharan mineral dust to the tropical northeast
1036 Atlantic Ocean: an intercomparison of methods, *Atmos Chem Phys*, 14, 2245-2266, DOI
1037 10.5194/acp-14-2245-2014, 2014.

1038 Nunes, T., personal communication, 2013.

1039 O'Dowd, C. D., Facchini, M. C., Cavalli, F., Ceburnis, D., Mircea, M., Decesari, S., Fuzzi, S.,
1040 Yoon, Y. J., and Putaud, J. P.: Biogenically driven organic contribution to marine aerosol,
1041 *Nature*, 431, 676-680, Doi 10.1038/Nature02959, 2004.

1042 O'Dowd, C. D., and De Leeuw, G.: Marine aerosol production: a review of the current
1043 knowledge, *Philos T R Soc A*, 365, 1753-1774, DOI 10.1098/rsta.2007.2043, 2007.

1044 Ohde, T., and Siegel, H.: Biological response to coastal upwelling and dust deposition in the area
1045 off Northwest Africa, *Cont Shelf Res*, 30, 1108-1119, DOI 10.1016/j.csr.2010.02.016, 2010.

1046 Paatero, P.: The multilinear engine - A table-driven, least squares program for solving multilinear
1047 problems, including the n-way parallel factor analysis model, *Journal of Computational and*
1048 *Graphical Statistics*, 8, 854-888, doi 10.2307/1390831, 1999.

1049 Pavuluri, C. M., Kawamura, K., Kikuta, M., Tachibana, E., and Aggarwal, S. G.: Time-resolved
1050 variations in the distributions of inorganic ions, carbonaceous components, dicarboxylic acids
1051 and related compounds in atmospheric aerosols from Sapporo, northern Japan during
1052 summertime, *Atmos Environ*, 62, 622-630, DOI 10.1016/j.atmosenv.2012.08.063, 2012.

1053 Quinn, P. K., Charlson, R. J., and Bates, T. S.: Simultaneous observations of ammonia in the
1054 atmosphere and ocean, *Nature*, 335, 336-338, Doi 10.1038/335336a0, 1988.

1055 Quinn, P. K., and Bates, T. S.: Regional aerosol properties: Comparisons of boundary layer
1056 measurements from ACE 1, ACE 2, aerosols99, INDOEX, ACE asia, TARFOX, and NEAQS, *J*
1057 *Geophys Res-Atmos*, 110, Artn D14202 Doi 10.1029/2004jd004755, 2005.

1058 Radhi, M., Box, M. A., Box, G. P., Mitchell, R. M., Cohen, D. D., Stelcer, E., and Keywood, M.
1059 D.: Optical, physical and chemical characteristics of Australian continental aerosols: results from
1060 a field experiment, *Atmos Chem Phys*, 10, 5925-5942, DOI 10.5194/acp-10-5925-2010, 2010.

1061 Raes, F., Liao, H., Chen, W. T., and Seinfeld, J. H.: Atmospheric chemistry-climate feedbacks, *J*
1062 *Geophys Res-Atmos*, 115, Artn D12121 Doi 10.1029/2009jd013300, 2010.

1063 Read, K. A., Mahajan, A. S., Carpenter, L. J., Evans, M. J., Faria, B. V. E., Heard, D. E.,
1064 Hopkins, J. R., Lee, J. D., Moller, S. J., Lewis, A. C., Mendes, L., McQuaid, J. B., Oetjen, H.,
1065 Saiz-Lopez, A., Pilling, M. J., and Plane, J. M. C.: Extensive halogen-mediated ozone destruction
1066 over the tropical Atlantic Ocean, *Nature*, 453, 1232-1235, Doi 10.1038/Nature07035, 2008.

1067 Reid, E. A., Reid, J. S., Meier, M. M., Dunlap, M. R., Cliff, S. S., Broumas, A., Perry, K., and
1068 Maring, H.: Characterization of African dust transported to Puerto Rico by individual particle and
1069 size segregated bulk analysis, *J Geophys Res-Atmos*, 108, Artn 8591 Doi 10.1029/2002jd002935,
1070 2003.

1071 Rijkenberg, M. J. A., Powell, C. F., Dall'Osto, M., Nielsdottir, M. C., Patey, M. D., Hill, P. G.,
1072 Baker, A. R., Jickells, T. D., Harrison, R. M., and Achterberg, E. P.: Changes in iron speciation
1073 following a Saharan dust event in the tropical North Atlantic Ocean, *Mar Chem*, 110, 56-67, DOI
1074 10.1016/j.marchem.2008.02.006, 2008.

1075 Rinaldi, M., Decesari, S., Carbone, C., Finessi, E., Fuzzi, S., Ceburnis, D., O'Dowd, C. D.,
1076 Sciare, J., Burrows, J. P., Vrekoussis, M., Ervens, B., Tsigaridis, K., and Facchini, M. C.:
1077 Evidence of a natural marine source of oxalic acid and a possible link to glyoxal, *J Geophys Res-*
1078 *Atmos*, 116, D16204 Doi10.1029/2011jd015659, 2011.

1079 Schepanski, K., Tegen, I., and Macke, A.: Saharan dust transport and deposition towards the
1080 tropical northern Atlantic, *Atmos Chem Phys*, 9, 1173-1189, 2009.

1081 Schulz, M., Prospero, J. M., Baker, A. R., Dentener, F., Ickes, L., Liss, P. S., Mahowald, N. M.,
1082 Nickovic, S., Garcia-Pando, C. P., Rodriguez, S., Sarin, M., Tegen, I., and Duce, R. A.:
1083 Atmospheric transport and deposition of mineral dust to the ocean: Implications for research
1084 needs, *Environ Sci Technol*, 46, 10390-10404, Doi 10.1021/Es300073u, 2012.

1085 Sciare, J., Oikonomou, K., Cachier, H., Mihalopoulos, N., Andreae, M. O., Maenhaut, W., and
1086 Sarda-Esteve, R.: Aerosol mass closure and reconstruction of the light scattering coefficient over
1087 the Eastern Mediterranean Sea during the MINOS campaign, *Atmos Chem Phys*, 5, 2253-2265,
1088 2005.

1089 Sciare, J., Favez, O., Sarda-Esteve, R., Oikonomou, K., Cachier, H., and Kazan, V.: Long-term
1090 observations of carbonaceous aerosols in the Austral Ocean atmosphere: Evidence of a biogenic
1091 marine organic source, *J Geophys Res-Atmos*, 114, Artn D15302 Doi 10.1029/2009jd011998,
1092 2009.

1093 Sullivan, R. C., Guazzotti, S. A., Sodeman, D. A., Tang, Y. H., Carmichael, G. R., and Prather,
1094 K. A.: Mineral dust is a sink for chlorine in the marine boundary layer, *Atmos Environ*, 41, 7166-
1095 7179, DOI 10.1016/j.atmosenv.2007.05.047, 2007.

1096 Tesche, M., Gross, S., Ansmann, A., Muller, D., Althausen, D., Freudenthaler, V., and Esselborn,
1097 M.: Profiling of Saharan dust and biomass-burning smoke with multiwavelength polarization
1098 Raman lidar at Cape Verde, *Tellus B*, 63, 649-676, DOI 10.1111/j.1600-0889.2011.00548.x,
1099 2011.

1100 Tilgner, A., and Herrmann, H.: Radical-driven carbonyl-to-acid conversion and acid degradation
1101 in tropospheric aqueous systems studied by CAPRAM, *Atmos Environ*, 44, 5415-5422, DOI
1102 10.1016/j.atmosenv.2010.07.050, 2010.

1103 Turpin, B. J., Saxena, P., and Andrews, E.: Measuring and simulating particulate organics in the
1104 atmosphere: problems and prospects, *Atmos Environ*, 34, 2983-3013, 2000.

1105 van Pinxteren, D., Brüggemann, E., Gnauk, T., Müller, K., Thiel, C., and Herrmann, H.: A GIS
1106 based approach to back trajectory analysis for the source apportionment of aerosol constituents
1107 and its first application, *J Atmos Chem*, 67, 1-28, DOI 10.1007/s10874-011-9199-9, 2010.

1108 Virkkula, A., Teinila, K., Hillamo, R., Kerminen, V. M., Saarikoski, S., Aurela, M., Viidanoja, J.,
1109 Paatero, J., Koponen, I. K., and Kulmala, M.: Chemical composition of boundary layer aerosol
1110 over the Atlantic Ocean and at an Antarctic site, *Atmos Chem Phys*, 6, 3407-3421, 2006.

1111 Warneck, P.: In-cloud chemistry opens pathway to the formation of oxalic acid in the marine
1112 atmosphere, *Atmos Environ*, 37, 2423-2427, Doi 10.1016/S1352-2310(03)00136-5, 2003.

1113 Williams, J., de Reus, M., Krejci, R., Fischer, H., and Strom, J.: Application of the variability-
1114 size relationship to atmospheric aerosol studies: estimating aerosol lifetimes and ages, *Atmos*
1115 *Chem Phys*, 2, 133-145, 2002.

1116 Yao, X. H., Fang, M., and Chan, C. K.: Size distributions and formation of dicarboxylic acids in
1117 atmospheric particles, *Atmos Environ*, 36, 2099-2107, 2002.

1118 Yao, X. H., and Zhang, L. M.: Chemical processes in sea-salt chloride depletion observed at a
1119 Canadian rural coastal site, *Atmos Environ*, 46, 189-194, DOI 10.1016/j.atmosenv.2011.09.081,
1120 2012.

1121

1122

1123 Table 1: HV-Filters collected at the CVAO from 2007 to 2011.

	2007	2008	2009	2010	2011
Total amount	105	105	154	148	159
72-hour-samples	45	69	66	105	85
24-hour-samples during intensive campaigns	60	36	88	43	74
Collected at 32m	105	105	132	50	159
Collected at 4m			22	98	

1124

1125

1126

1127 Table 2 Minimum, maximum, 5 year average and standard deviations ($\mu\text{g}/\text{m}^3$) of PM_{10}
 1128 aerosol components at CVAO.

Components	Min	Max	Mean	Median	Stdev
mass load	4.00	601.83	47.20	30.10	55.50
Dust	0.00	575.56	25.90	9.70	51.10
Sea salt	0.71	39.67	11.00	10.71	5.10
Cl^-	0.35	21.17	5.70	5.43	2.70
Br^-	Bdl	0.25	0.005	0.003	0.01
NO_3^-	0.14	3.76	1.10	1.00	0.60
SO_4^{2-}	0.31	7.38	2.50	2.33	1.20
$\text{C}_2\text{O}_4^{2-}$	Bdl	0.46	0.08	0.06	0.10
Na^+	0.25	12.74	3.70	3.72	1.70
NH_4^+	Bdl	0.76	0.09	0.05	0.10
K^+	Bdl	0.86	0.13	0.13	0.10
Mg^{2+}	0.05	1.34	0.40	0.37	0.20
Ca^{2+}	Bdl	4.44	0.64	0.46	0.60
OM (OC*2)	Bdl	6.67	1.02	0.67	1.04
EC	Bdl	1.32	0.13	0.08	0.16

1129 Bdl : below detection limit.

1130 Table 3: Seasonality of PM₁₀ particle mass concentration collected with DHA-80 HV-filter
 1131 sampler between January 2007 and November 2011 on top of the tower*.

season	Mar - May	Jun – Aug	Sep – Nov	Dec - Feb	Total
Mass: >200 µg/m ³	2	0	1	15	18
Mass: 90-200 µg/m ³	7	4	10	22	43
Mass: 20-90 µg/m ³	62	98	91	98	349
Mass: <20 µg/m ³	47	22	19	41	129
Total samples	118	124	121	176	539

1132 *Samples collected between 23rd of October 2009 and 09th of July 2010 were not included here
 1133 because of the lower sampling height on the container roof.

1134

1135 Table 4: Comparison of published averaged oxalate concentration in PM₁₀ aerosols with
 1136 the results of this study

Sampling site	Sampling interval	Oxalate [µg/m ³]	Reference
CVAO, marine non-polluted	Winters 2007-2011	0.07±0.06	This study
CVAO, marine non-polluted	Summers 2007-2011	0.06±0.05	This study
CVAO, continentally influenced	2007-2011	0.12±0.06 (Africa) 0.12±0.05 (Europe)	This study
Amsterdam Island	2003-2007	0.0003 – 0.017	(Rinaldi et al. 2011)
Mace Head	2006	0.0027 – 0.039	
Tropical to Northwest Pacific	Sep-Dec 1990	0.040	(Kawamura and Sakaguchi, 1999)
Tropical Atlantic	April 1996	0.052±0.030	(Johansen et al., 2000)
Atlantic Ocean 25°N - 4°S	November 1999	0.074±0.048	(Virkkula et al., 2006)
Hong Kong	December 2000	0.35	(Yao et al., 2002)
Sapporo , Japan	August 2005	0.196	(Pavuluri et al., 2012)

1137

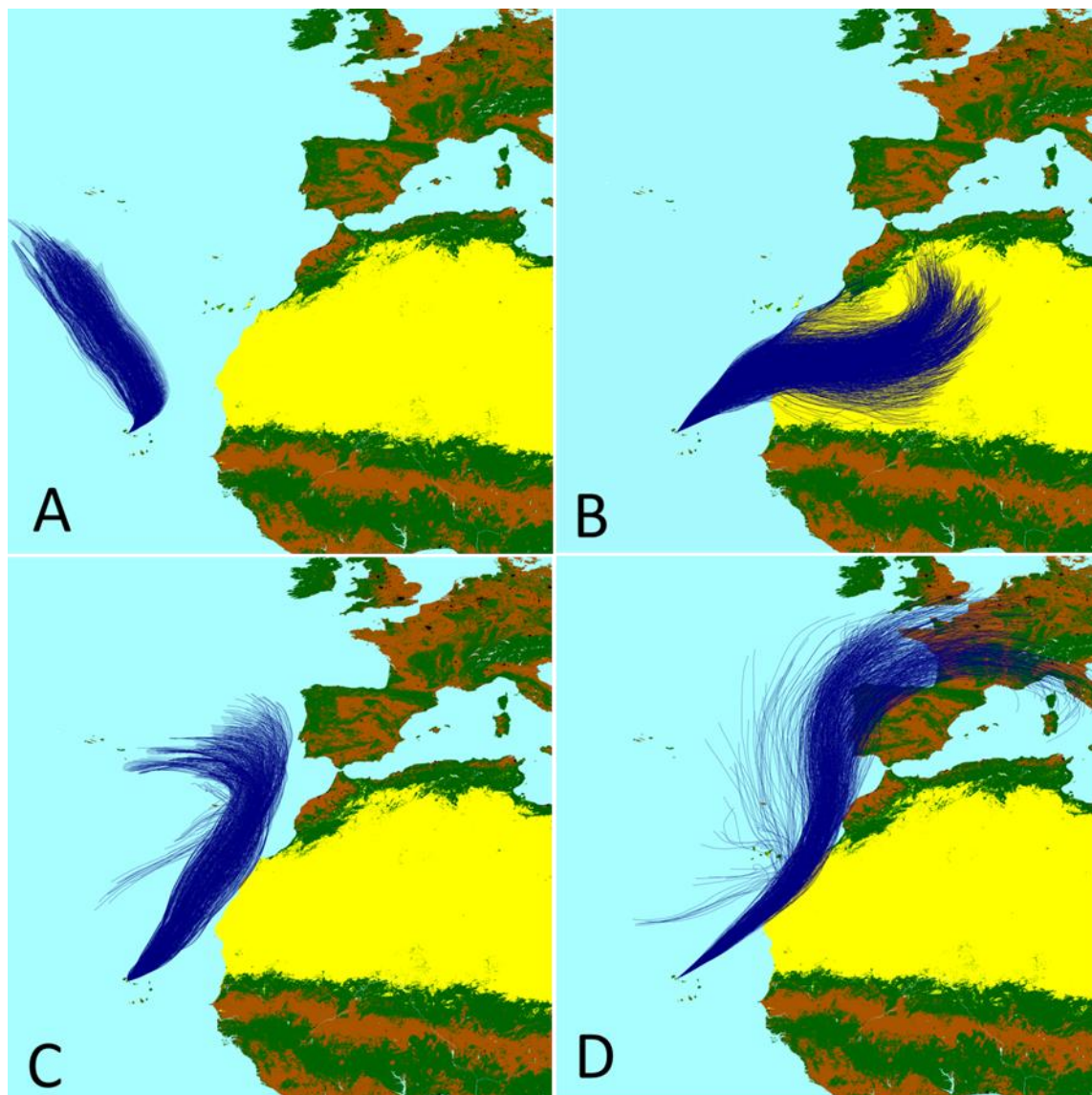
1138 Table 5: Comparison of major non-sea-salt components and halogenide depletion (mean
 1139 values and standard deviation as an estimation of the scatter) in four classes of
 1140 particulate matter collected at the tower at the CVAO.
 1141

Concentration [$\mu\text{g}/\text{m}^3$]	Dust – rich Saharan aerosol	Marine aerosol summer	Marine aerosol Winter	Europe influenced aerosol	Mean of all samples
Mass concentration (N)	173.4 \pm 95.5 (56)	16.4 \pm 4.5 (43)	14.5 \pm 5.8 (33)	35.3 \pm 13.6 (55)	47.3 \pm 55.5 (539)
Dust (estimated)	144.6 \pm 95.8	2.7 \pm 2.6	2.0 \pm 4.1	6.1 \pm 9.9	25.8 \pm 51.4
OM	3.16 \pm 1.69	0.58 \pm 0.35	1.04 \pm 0.7	0.86 \pm 0.47	1.01 \pm 1.04
EC	0.38 \pm 0.32	0.05 \pm 0.05	0.04 \pm 0.03	0.12 \pm 0.08	0.13 \pm 0.16
Nitrate	1.75 \pm 0.69	0.58 \pm 0.28	0.48 \pm 0.22	1.36 \pm 0.49	1.10 \pm 0.56
Non-sea-salt Sulfate	2.46 \pm 1.05	1.01 \pm 0.45	0.47 \pm 0.31	1.76 \pm 0.99	1.54 \pm 1.04
Ammonium	0.064 \pm 0.08	0.07 \pm 0.05	0.036 \pm 0.	0.165 \pm 0.18	0.088 \pm 0.10
Time over Ocean [h]	<48	>120	>120	>72	--
Chloride depletion [%]	8.8 \pm 8.5	26 \pm 15	20 \pm 13	30 \pm 12	16 \pm 10
Bromide depletion [%]	62 \pm 42	88 \pm 13	83 \pm 20	87 \pm 11	80 \pm 20
[Cl ⁻] / [Na ⁺] (1.17 in sea water)	1.06	0.95	1.03	0.80	
[Cl ⁻ + NO ₃ ⁻] / [Na ⁺]	1.19	1.02	1.10	0.91	

1142

1143

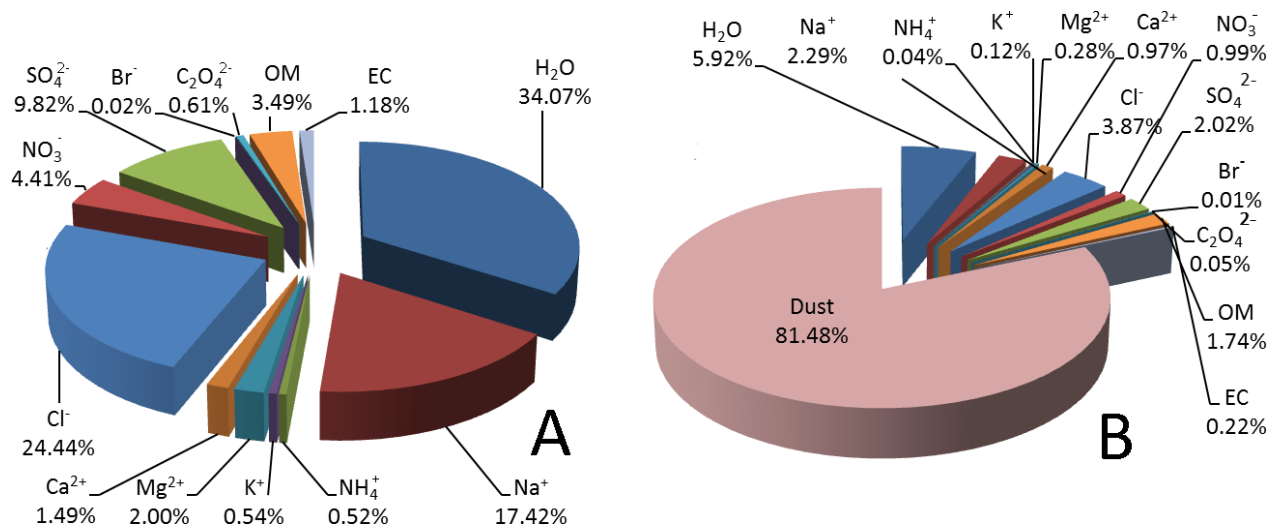
1144
1145



1146
1147

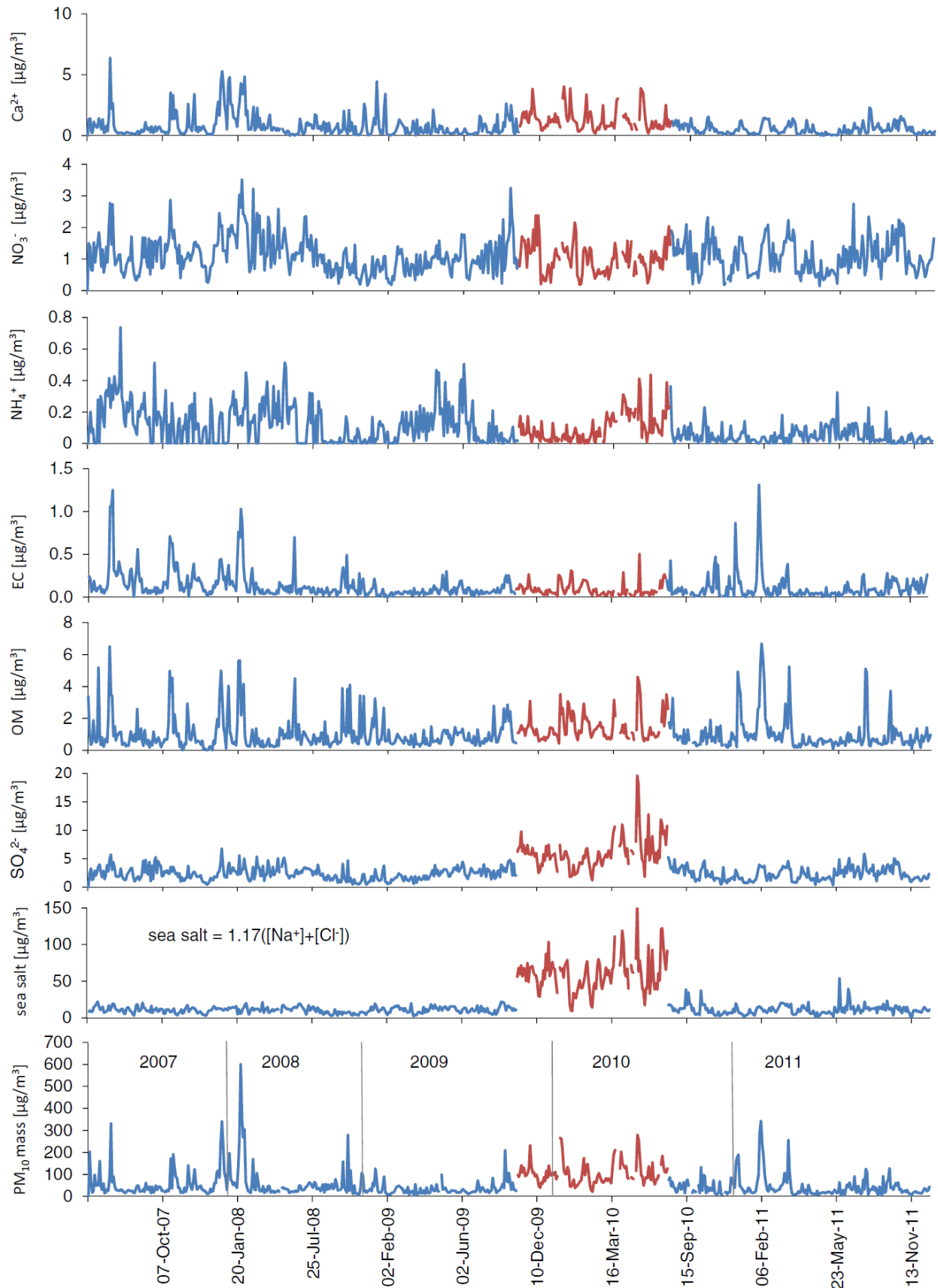
1148 Figure 1. Typical 96 hour air mass back trajectory ensembles calculated for CVAO during the
1149 routine filter sampling periods, aerosol type and PM_{10} mass concentration are given in
1150 parentheses: A) 02-May-2011: marine air mass from Northern Atlantic Ocean (mass, $m=8.28$
1151 $\mu\text{g}/\text{m}^3$); B) 14-Jan-2011: Saharan air mass (dust loaded, $m=155.04 \mu\text{g}/\text{m}^3$); C) 12-Jul-2008:
1152 slightly polluted air mass from the Northwest-African coast and the Canary Islands, $m=21.61$
1153 $\mu\text{g}/\text{m}^3$. D) 02-Feb-2011: Air mass from Europe crossing the coast-line of NW Africa and the
1154 Canary Islands (anthropogenically influenced, $m=64.89 \mu\text{g}/\text{m}^3$);

1155

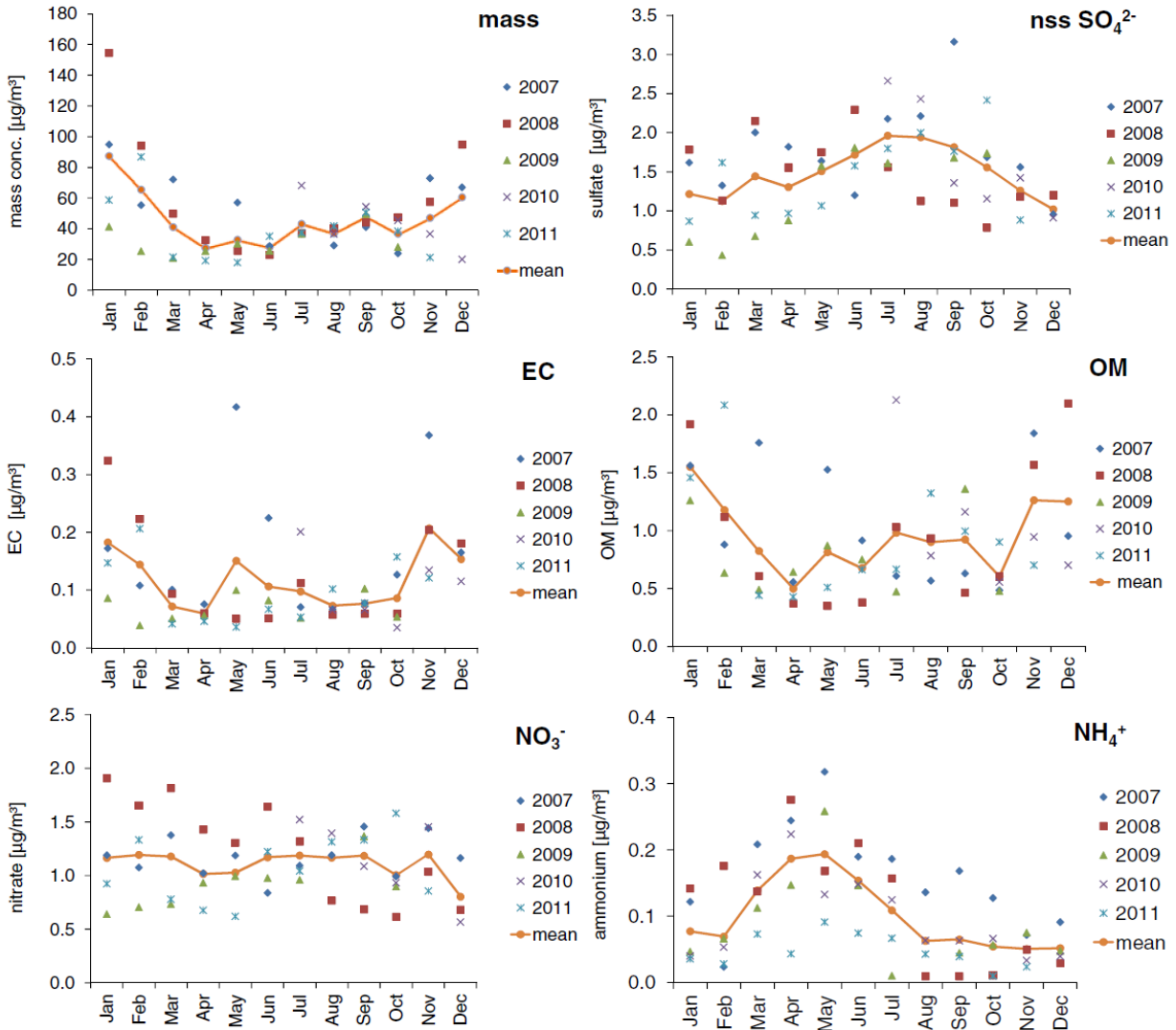


1156
 1157
 1158
 1159
 1160
 1161
 1162

Figure 2. Averaged PM₁₀ constitution for 183 marine samples (A) and 49 mineral dust dominated aerosol samples (B) collected at 32 m on top of the tower.

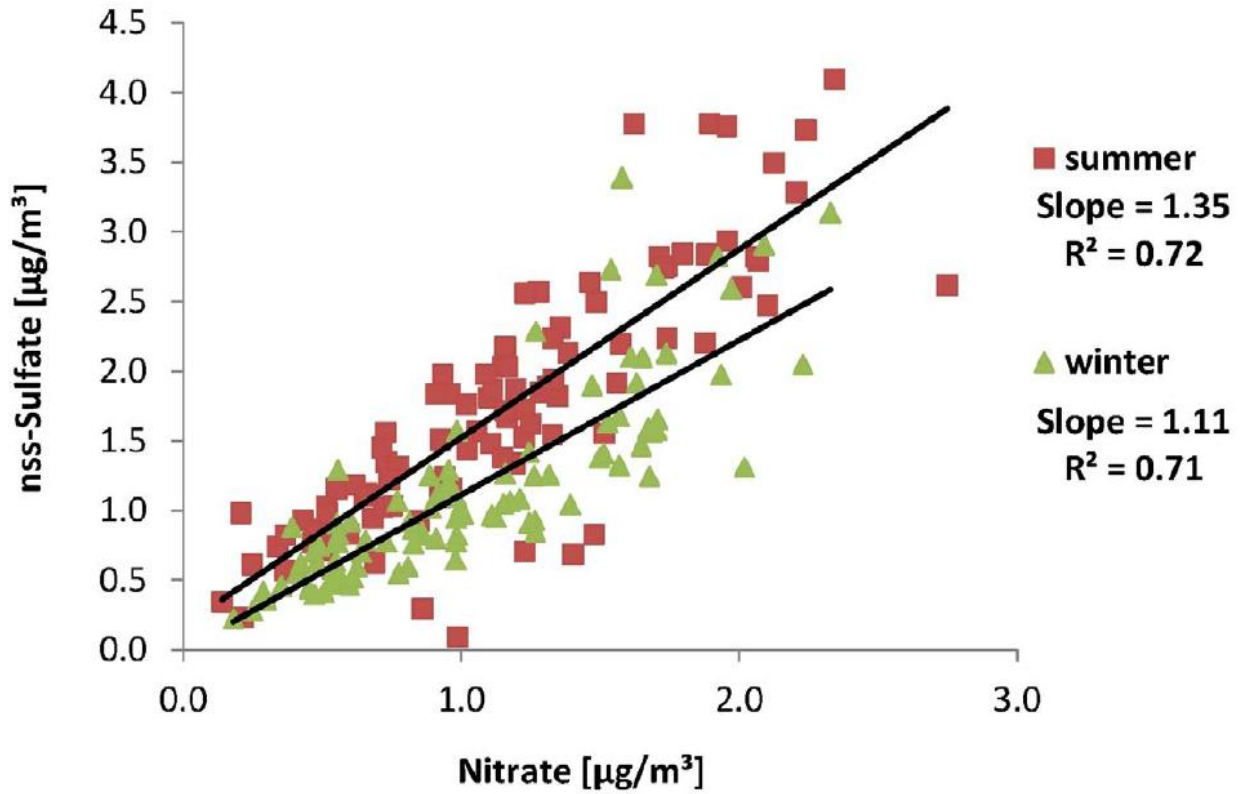


1164 Figure 3. Time series of mass concentration and major PM₁₀ aerosol components in filter samples
 1165 collected during the five years from 2007 to 2011. During the period from 23 October 2009 till
 1166 09 July 2010 (red line) all samples were collected on top of a storage container with an inlet
 1167 height of 4 m above ground, all other samples were collected on top of the tower with an inlet
 1168 height of 32m above ground.
 1169



1170
 1171
 1172 Figure 4. Annual variability and monthly mean of PM₁₀ mass concentration, non-sea-salt sulfate,
 1173 elemental carbon (EC), organic matter (OM), nitrate, and ammonium during the five years of
 1174 measurements for samples collected on the tower.
 1175

1176



1177

1178

1179 Figure 5. Correlation between nitrate and nss-sulfate between Summer and Winter in samples
1180 collected from July 2010 to November 2011.

1181

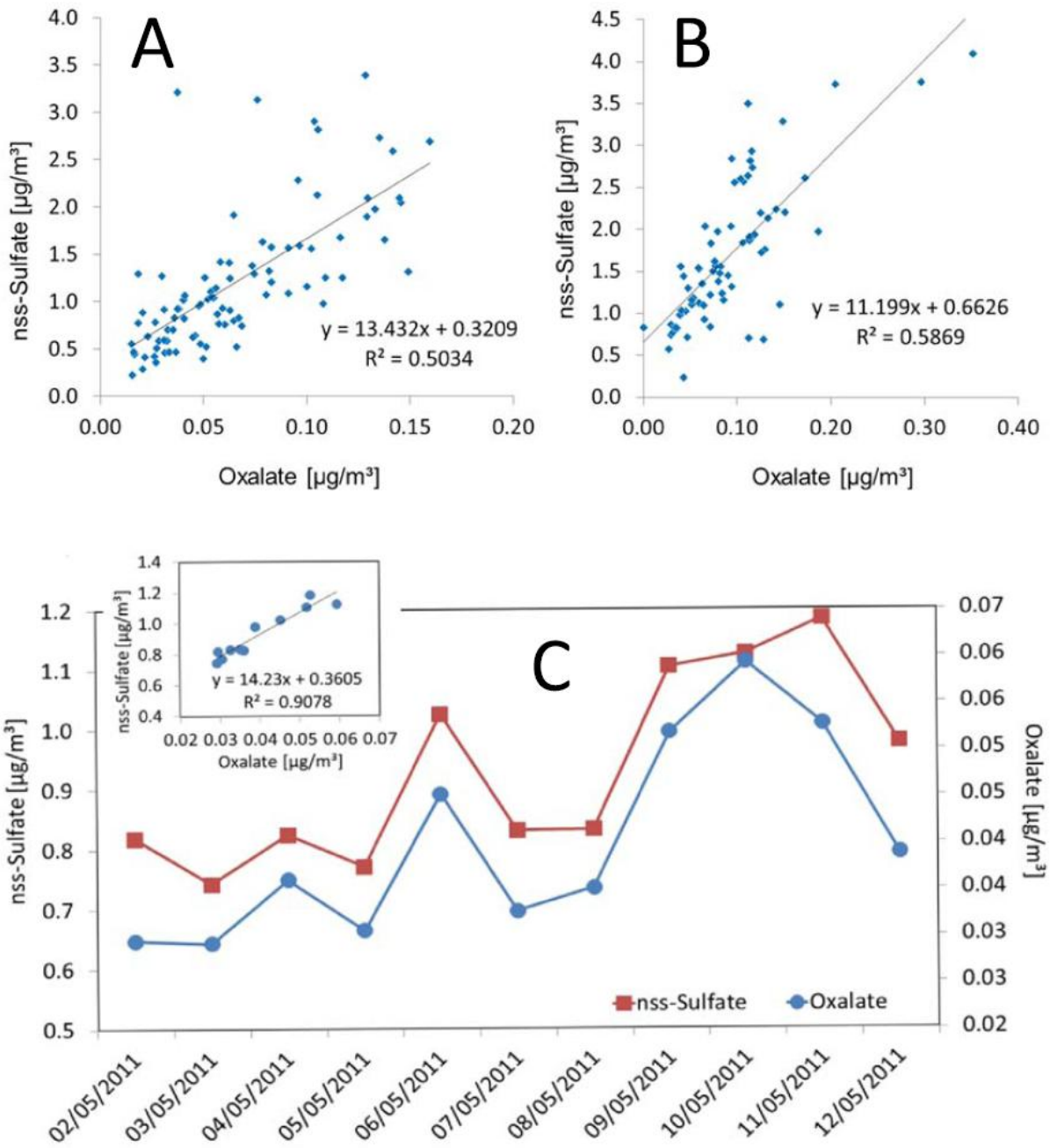
1182

1183

1184

1185

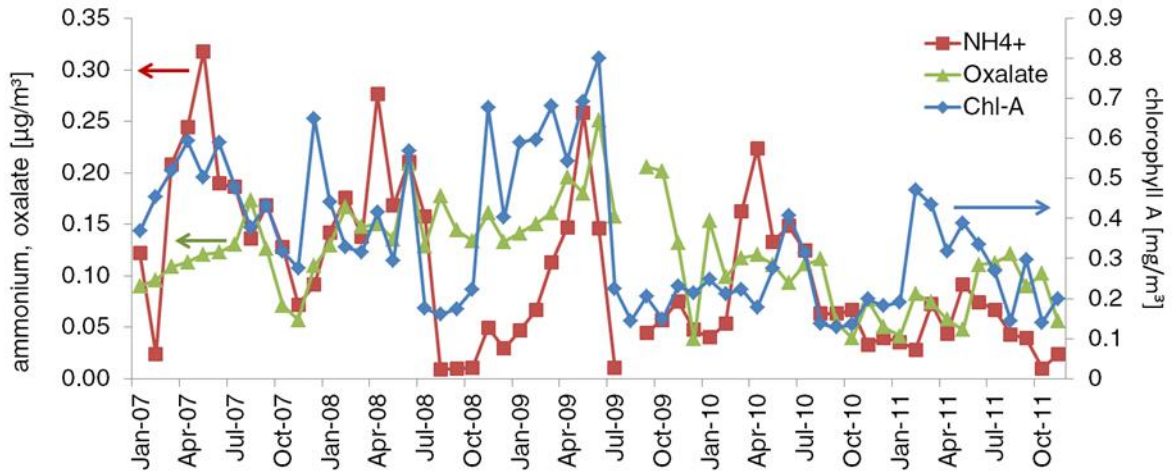
1186



1187
 1188
 1189
 1190
 1191
 1192
 1193

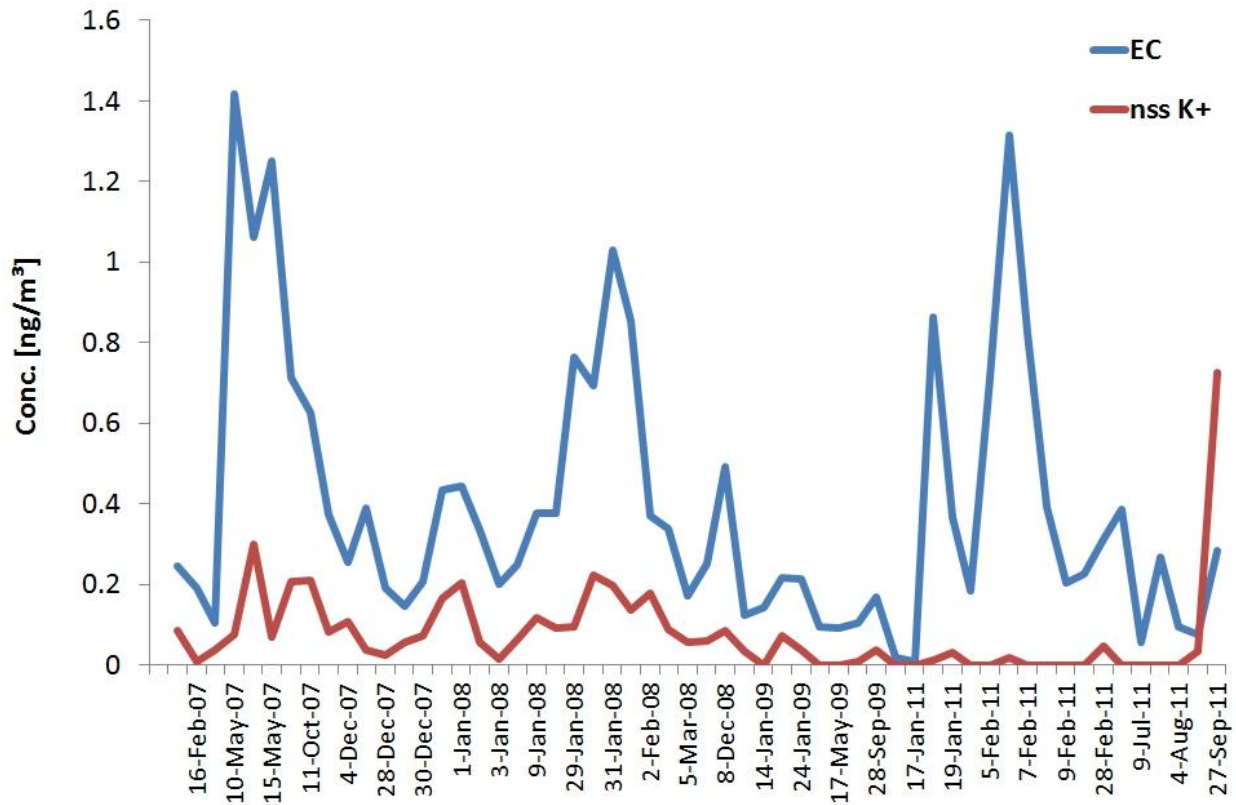
Figure 6. Correlation between nss-sulfate and oxalate in filter samples during 2010/2011, above (a) winter, (b) summer, and below (c) concentration and correlation during a marine clean air episode in May 2011.

1194
1195
1196



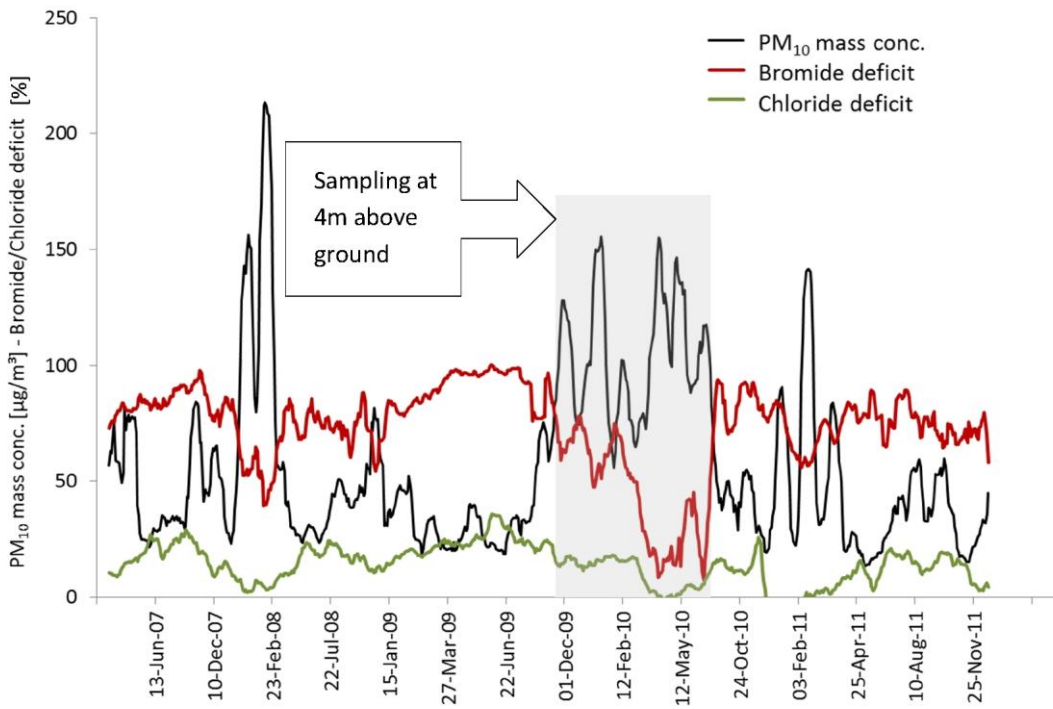
1197
1198
1199
1200
1201
1202
1203

Figure 7. Monthly mean of chlorophyll A in the tropical NE Atlantic (selected area for averaging: Lat(16.985, 24.895), Lon(-24.87, -18.278)) , oxalate and ammonium in PM₁₀ aerosol samples collected at the CVAO.



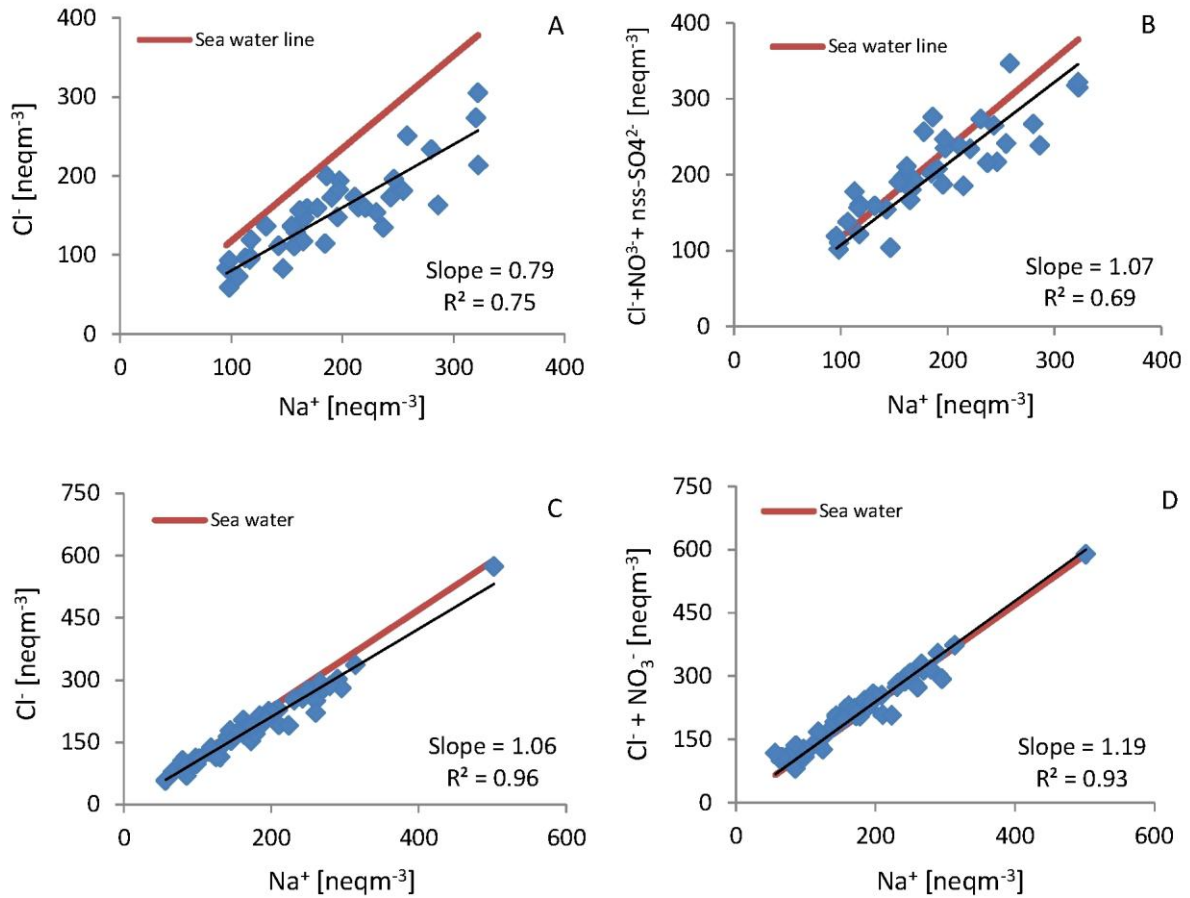
1204
 1205
 1206
 1207
 1208

Figure 8. Time series of nss-potassium (nss-K⁺) and elemental carbon (EC) measured during air mass inflow from Africa revealing similar temporal variations.



1209
 1210
 1211
 1212
 1213
 1214
 1215
 1216
 1217
 1218
 1219
 1220
 1221

Figure 9. Variability of bromide and chloride deficit in comparison to the total PM₁₀ mass concentration (all curves represent 10 sample running mean) and the season.



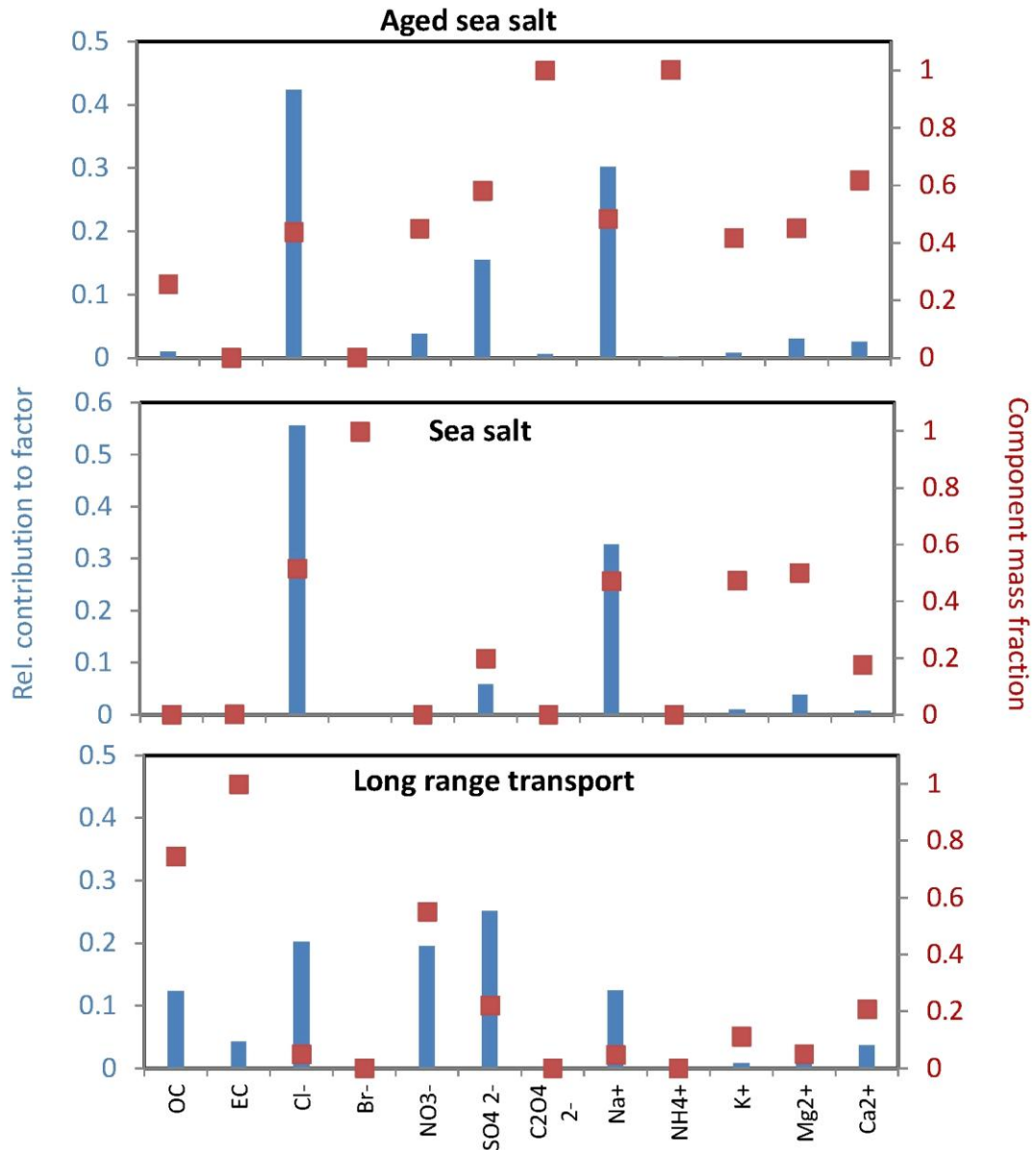
1222

1223

1224 Figure 10. Scatter plots between a) Na^+ and Cl^- , b) Na^+ and $\text{Cl}^- + \text{NO}_3^- + \text{nss-SO}_4^{2-}$ during summer
 1225 marine air mass inflow and c) Na^+ and Cl^- , d) Na^+ and $\text{Cl}^- + \text{NO}_3^-$ during Saharan dust events at
 1226 the CVAO.

1227

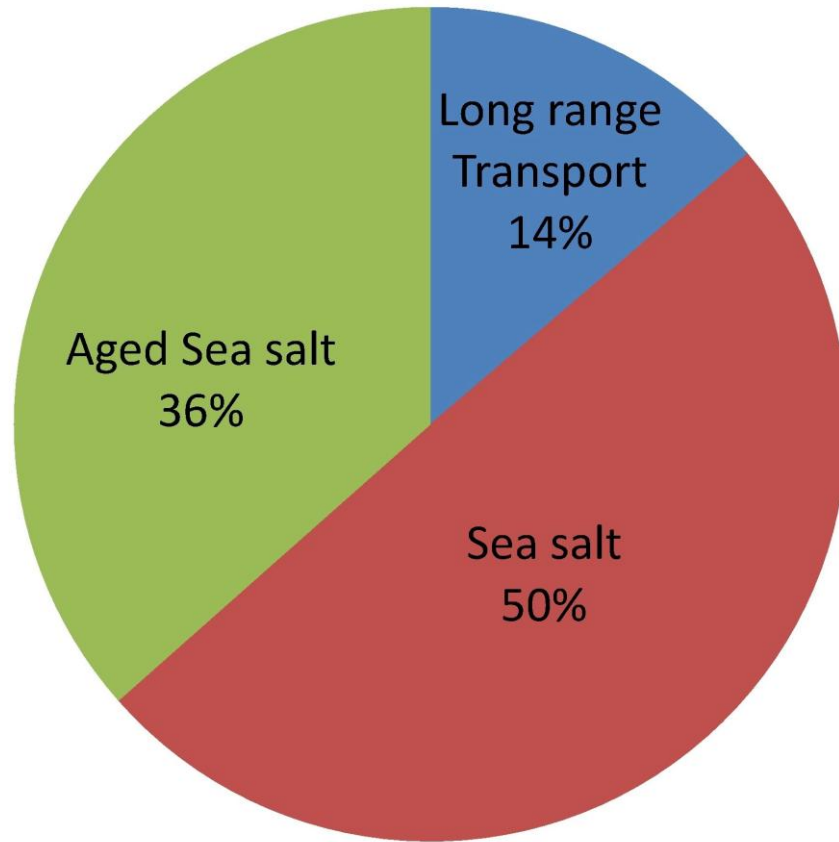
1228



1229
 1230
 1231
 1232
 1233
 1234
 1235
 1236
 1237

Figure 11. Source profiles identified from measured PM₁₀ components at CVAO. Results are from 671 analyzed filters. The relative contribution of each species to a given factor is represent as blue bars while the relative contribution of each factor to the total specie concentration is represented as red square (right axis).

1238



1239

1240

1241 Figure 12. Average contribution of each source to the total analyzed species

1242

1243

1244

1245

1246

1247

1248